Hybrid Transceiver Design and Optimal Power Allocation for the Cognitive mmWave Multiuser MIMO Downlink Relying on Limited Feedback

Jitendra Singh, *Student Member, IEEE,* Indranil Chatterjee, *Student Member, IEEE,* Suraj Srivastava, *Graduate Student Member, IEEE,* Abhishek Agrahari, Aditya K. Jagannatham, *Member, IEEE* Lajos Hanzo, *Life Fellow, IEEE*

***Abstract*—A hybrid transceiver architecture is conceived for a cognitive radio (CR) aided millimeter wave (mmWave) multiuser (MU) multiple-input multiple-output (MIMO) downlink system relying on multiple radio frequency (RF) chains both at the CR base station (CBS) and the secondary users (SUs). To begin with, a hybrid transceiver design algorithm is proposed for the CBS and SUs, to maximize the sum spectral efficiency (SE) by decoupling the hybrid transceiver into a blind minimum mean squared error (MMSE) receiver combiner (RC) and optimal-capacity two-stage hybrid transmit precoder (TPC) components. These RC-weights and TPC-weights are subsequently found by using the popular simultaneous orthogonal matching pursuit (SOMP) technique. A closed-form solution is derived for the optimal power allocation that maximizes the sum SE under the associated interference and transmit power constraints. To achieve user fairness, we also propose an optimal power allocation scheme for maximizing the geometric mean (GM) of the SU rates. Finally, a low-complexity limited feedback aided hybrid transceiver is designed, which relies on the random vector quantization (RVQ) technique. Our simulation results demonstrate that an improved SE is achieved in comparison to the state-of-the-art techniques.**

***Index Terms*—Millimeter wave, cognitive radio, multiple-input multiple-output (MIMO), hybrid beamforming, sparse reconstruction.**

I. INTRODUCTION

MILLIMETER wave (mmWave) communication technology, which exploits the large slabs of bandwidth available in $30-300$ GHz band, provides the wireless industry an exceptional opportunity to support ultra-high data rates on the order of Gbps in beyond 5G (B5G) wireless networks [1], [2]. On the other hand, the inevitable proliferation of connected devices in B5G can potentially lead to spectral congestion. In such a system, advanced spectrum sharing-based cognitive radio (CR) technology, together with mmWave communication, is likely to play a vital role in enhancing the overall system spectral efficiency (SE). However, communication in the mmWave regime is a challenging task due to the severe propagation, penetration losses and signal blockages [3]. Thankfully, the short wavelength of signals in the mmWave band enables the dense packing of a large number of antenna elements, which leads to a high beamforming gain that can be exploited to overcome the above losses [2].This also presents an excellent opportunity to harness CR technology, wherein the mmWave spectrum allocated to licensed primary users (PUs) can be accessed opportunistically by the unlicensed secondary users (SUs).

In such mmWave multiuser (MU) multiple-input-multiple-output (MIMO) CR systems, the design of suitable precoding/combining techniques is an immensely challenging task due to the power and hardware constraints coupled with the stringent interference threshold constraints set by the PUs. Furthermore, the conventional fully-digital transmit precoding (TPC)/receiver combining (RC) schemes used in sub-6 GHz MIMO systems are unsuited for the mmWave band as they require a separate radio frequency (RF) chain for each antenna, which leads to high hardware cost and power consumption [2], [4]. To avoid the above shortcomings, the recently proposed hybrid MIMO architecture [3]–[8] has shown significant promise in attaining the much needed beamforming gain using a remarkably low number of RF chains. Hence, hybrid TPC/RC design along with optimal power allocation holds the key toward practical realization of mmWave MIMO CR systems, which forms the focus of this work. A brief literature review of research in this area is presented next.

A. Literature review

The initial investigations in [9]–[18] demonstrated that mmWave networks can efficiently share the available spectrum by relying on bespoke spectrum access techniques. Specifically, [9] provided a comprehensive survey of spectrum sharing paradigms in 5G CR networks. *Rebato et al.,* in their seminal work in [14], conceived a hybrid spectrum sharing scheme for mmWave CR systems wherein the mmWave spectrum is pooled among multiple cellular operators. Additionally, [15] provided a mathematical framework for multi-operator spectrum-shared mmWave networks and analyzed the coverage probability in such systems. Furthermore, *Li et al.* [16] proposed a decentralized reinforcement learning-based algorithm for maximizing the throughput of dynamic spectrum-sharing enabled ultradense mmWave CR systems. In contrast to [16], the authors of [17] proposed a data-driven approach to maximize the throughput of spectrum-sharing enabled mmWave networks, which is also robust to insufficient signaling and missing CSI. The authors of [18] designed various carrier sensing protocols for distributed interference management in spectrum-shared mmWave networks.

L. Hanzo would like to acknowledge the financial support of the Engineering and Physical Sciences Research Council projects EP/W016605/1 and EP/P003990/1 (COALESCE) as well as of the European Research Council's Advanced Fellow Grant QuantCom (Grant No. 789028).

J. Singh, I. Chatterjee, S. Srivastava, and A. K. Jagannatham are with the Department of Electrical Engineering, Indian Institute of Technology Kanpur, Kanpur, UP 208016, India (e-mail: jitend@iitk.ac.in; indrac@iitk.ac.in; ssrivast@iitk.ac.in; adityaj@iitk.ac.in).

A. Agrahari is with Radisys India Private Limited, Bangalore, 560103, India (e-mail: abhishekagrahari@gmail.com).

L. Hanzo is with the School of Electronics and Computer Science, University of Southampton, Southampton SO17 1BJ, U.K. (e-mail: lh@ecs.soton.ac.uk).

However, one must note that the benefits of spectrum sharing are strongly influenced by coordination techniques, which are closely related to the underlying architecture [19]–[24]. In [19], the authors maximized the throughput and fairness of the users by employing joint beamforming, coordination and base station (BS) association, in the multi-operator spectrum-shared mmWave downlink of a cellular network. Along similar lines, the authors of [20] maximized the geometric mean (GM) of the user rates for ensuring fairness in resource allocation.

Furthermore, *Park et al.* [21] employed inter-operator coordination to construct the complementary cumulative distribution function (CCDF) of the rate and concluded that the coordination is effective in spectrum sharing when the operators are densely tessellated and form wide beams. It is worth noting that the studies [23], [24] show the negative impact of the shared spectrum on the achievable SE when the interference power is not regulated. To avoid this, the authors of [25] proposed spectrum sharing microwave systems relying on a single BS having a single RF chain and proposed a phase-only TPC to limit the interference. *Vázquez et al.* [26], proposed a hybrid beamforming solution for spectrum-sharing backhaul networks that maximize the array gain at the intended receiver, while forcing the array gain of the unintended users to lie below a maximum tolerable threshold. Furthermore, the very recent treatise [27] determined the hybrid transceiver architecture of mmWave MU MIMO CR systems for both the uplink and the downlink based on the alternating direction method of multipliers (ADMM). As a further advance, the authors of [28] extended the equal gain transmission-block diagonalization (EGT-BD) based two-stage transceiver design of [29] to mmWave MU MIMO CR systems by relying on optimal power allocation subject to a specific interference threshold. The analog TPC/RC was designed separately from the digital TPC/RC. Moreover, the authors of [30] investigated spectrum sharing over the mmWave band between cellular and WiGig users, and proposed an iterative channel allocation and hybrid beamforming algorithm that maximized the sum rate of cellular users while minimizing the interference to the WiGig network. Furthermore, the authors of [31], [32] investigated hybrid TPC designs for enhancing the physical layer security of mmWave CR systems.

Although, the contributions reviewed above and the references therein form a rich literature on mmWave MIMO CR systems, several shortcomings remain to be addressed. To begin with, for an mmWave MU MIMO CR system, the optimal power allocation has not been considered, even though it has a significant impact on the overall performance. Furthermore, the MUI cancellation techniques of the existing mmWave MU MIMO CR systems have been designed by considering only single RF chains at the users. The extension of this problem to multi antenna users each having multiple RF chains has not been addressed yet. Moreover, none of the existing studies have designed the hybrid TPC/RC using limited feedback in this context. These knowledge gaps motivate us to develop a hybrid transceiver for a mmWave MU MIMO CR system for supporting multi-antenna, multi-RF users, while also determining the optimal power allocation based on the available CSI and interference power constraints set by the PU for both the analog and limited feedback scenarios. Our novel contributions are boldly and explicitly contrasted to the existing literature in Table I. Our novel contributions are presented next in more detail.

B. Contributions of this work

1) The hybrid transceiver design problem is formulated to achieve the sum SE maximization of the mmWave MU MIMO CR downlink, while considering the interference power constraint set by the PU as well as the power and hardware constraints imposed by the mmWave hybrid MIMO architecture. In order to solve this challenging non-convex problem, the hybrid transceiver optimization problem is decoupled into blind MMSE-optimal hybrid RC design and optimal-capacity hybrid TPC design. Next, the MMSE combiner is designed for each SU via the efficient simultaneous orthogonal matching pursuit (SOMP) technique, considering the optimal fully-digital TPC with *blind* equal-power allocation to each stream at the CBS.
2) The associated sum SE maximization problem is formulated under both hardware and interference constraints, by exploiting the effective channel matrix of each SU, that comprises both the blind MMSE RC and the mmWave MIMO channel. A simplified two-stage hybrid TPC design procedure is also developed, which designs the RF and BB TPCs in the first and second stages, respectively.
3) Employing the RF TPC together with the BB TPCs, a closed-form solution is derived for the optimal power allocation to maximize the SE of the system. Furthermore, in order to achieve fairness, a power allocation solution is also derived to maximize the GM of the SU rates.
4) A low-complexity hybrid transceiver design is also developed for limited-feedback systems. Since this has a significantly reduced feedback overhead, it is eminently suited for practical mmWave MIMO CR systems.

C. Notation

$\mathbf{A}$, $\mathbf{a}$, and a represent a matrix, a vector, and a scalar quantity respectively; The ith column, (i,j)th element, and Hermitian of matrix $\mathbf{A}$ are denoted by $\mathbf{A}^{(i)}$, $\mathbf{A}(i,j)$, and $\mathbf{A}^H$, respectively; $||\mathbf{A}||_F$ denotes the the Frobenius norm of $\mathbf{A}$, whereas $|\mathbf{A}|$ represents its determinant; $\mathrm{Tr}(\mathbf{A})$ denotes its trace; $||\mathbf{a}||_p$ represents p-th norm of $\mathbf{a}$; $\mathrm{diag}(\mathbf{A})$ is a column vector formed by the diagonal entries of $\mathbf{A}$ whereas $\mathcal{D}(\mathbf{a})$ denotes a diagonal matrix with vector $\mathbf{a}$ on its main diagonal; The expectation operator is represented as $\mathbb{E}[\cdot]$; $\mathcal{R}(\mathbf{A})$ and $\mathcal{C}(\mathbf{A})$ denote the row and column spaces of the matrix $\mathbf{A}$; $\mathbf{I}_M$ denotes an $M \times M$ identity matrix; the symmetric complex Gaussian distribution of mean $\mathbf{a}$ and covariance matrix $\mathbf{A}$ is represented as $\mathcal{CN}(\mathbf{a}, \mathbf{A})$.

Table I: Summary of literature survey on mmWave MIMO CR systems

	[2]	[3]	[19]	[20]	[21]	[23]	[25]	[26]	[27]	[28]	[30]	Proposed
mmWave MIMO system	✓	✓	✓		✓	✓	✓	✓	✓	✓	✓	✓
Multiuser		✓	✓	✓	✓	✓	✓	✓	✓	✓	✓	✓
Multi RF chain users	✓								✓	✓		✓
CR system			✓			✓	✓	✓	✓	✓	✓	✓
Two-stage hybrid precoder		✓										✓
Hybrid MMSE combiner	✓								✓			✓
SOMP	✓											✓
Precoder/combiner using Codebook		✓			✓					✓		✓
ZF precoder/combiner			✓								✓	✓
Optimal power allocation					✓					✓	✓	✓
GM maximization				✓								✓
Limited feedback	✓	✓										✓

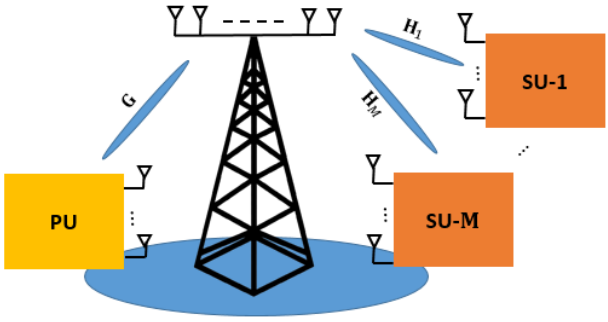

Figure 1: Block diagram of a mmWave MU-MIMO underlay cognitive radio system.

II. mmWave MU MIMO CR SYSTEM

A. System model

Consider a mmWave MU MIMO CR system operating in the underlay mode, where a CBS having N_{t} transmit antennas (TAs) and M_{t} RF chains is communicating to M SUs each having N_{r} receive antennas (RAs) and M_{r} RF chains in the presence of a PU, as shown in Fig. 1. Furthermore, as demonstrated in Fig. 2, in order to support multi-stream communication using an hybrid architecture, the number of RF chains M_{t} at the CBS is constrained to satisfy $MN_{\mathrm{s}} \leq M_{\mathrm{t}} \leq N_{\mathrm{t}}$, whereas for each SU we have $N_{\mathrm{s}} \leq M_{\mathrm{r}} \leq N_{\mathrm{r}}$, where N_{s} represents the number of parallel data streams per SU. This allows the CBS to apply the $M_{\mathrm{t}} \times MN_{\mathrm{s}}$ BB digital TPC $\mathbf{F}_{\mathrm{BB}}$ followed by an $N_{\mathrm{t}} \times M_{\mathrm{t}}$ RF TPC $\mathbf{F}_{\mathrm{RF}}$ comprising only analog phase shifters. At this point, it is important to note that this paper focuses on the hybrid transceiver design for SUs, which also operate in the same frequency band as the PU. Furthermore, the PU can apply TPC techniques independently of the secondary system depending on various metrics such as SE maximization, BER reduction, etc., assuming the SU's absence. Because the SUs must avoid violating the maximum tolerable interference imposed by the PU, the overall SE of the system suffers as a result of power constraints at the SUs.

Let $\mathbf{H}_m \in \mathbb{C}^{N_{\mathrm{r}} \times N_{\mathrm{t}}}, m = 1, \ldots M$, denote the mmWave MIMO channel matrix of all the links spanning from the CBS to the mth SU and $\mathbf{G} \in \mathbb{C}^{N_{\mathrm{r}} \times N_{\mathrm{t}}}$ represent the same between the CBS and the PU. By considering a narrowband block-fading channel model [3], [7], the signal $\mathbf{y}_m \in \mathbb{C}^{N_{\mathrm{r}} \times 1}$ received at the mth SU is given by

$$\begin{aligned}\mathbf{y}_m =& \mathbf{H}_m \mathbf{F}_{\mathrm{RF}} \mathbf{F}_{\mathrm{BB}} \mathcal{D}(\sqrt{\mathbf{p}})\mathbf{s} + \mathbf{n}_m \\ =& \mathbf{H}_m \mathbf{F}_{\mathrm{RF}} \mathbf{F}_{\mathrm{BB},m} \mathcal{D}(\sqrt{\mathbf{p}_m})\mathbf{s}_m \\ &+ \sum_{n=1, n\neq m}^{M} \mathbf{H}_m \mathbf{F}_{\mathrm{RF}} \mathbf{F}_{\mathrm{BB},n} \mathcal{D}(\sqrt{\mathbf{p}_n})\mathbf{s}_n + \mathbf{n}_m,\end{aligned} \tag{1}$$

where $\mathbf{s} = [\mathbf{s}_1^T, \mathbf{s}_2^T, \ldots, \mathbf{s}_M^T]^T \in \mathbb{C}^{MN_{\mathrm{s}} \times 1}$ denotes the symbol vector corresponding to all the SUs and each $\mathbf{s}_m \in \mathbb{C}^{N_{\mathrm{s}} \times 1}$ is the symbol vector corresponding to the mth SU having zero mean and covariance matrix $\mathbf{R}_{\mathrm{ss},m} = \mathbb{E}[\mathbf{s}_m \mathbf{s}_m^H] = \mathbf{I}_{N_{\mathrm{s}}}$. Furthermore, $\mathbf{p} = [\mathbf{p}_1^T, \ldots, \mathbf{p}_m^T, \ldots, \mathbf{p}_M^T]^T \in \mathbb{R}^{MN_{\mathrm{s}} \times 1}$ denote the power allocation vector, where $\mathbf{p}_m(i)$ signifies the power allocated to the ith stream at the mth SU. In the above, note that the analog TPC $\mathbf{F}_{\mathrm{RF}}$ is same for all the SUs, whereas the BB precoder $\mathbf{F}_{\mathrm{BB},m} \in \mathbb{C}^{M_{\mathrm{t}} \times N_{\mathrm{s}}}$ corresponds to the mth SU, so that $\mathbf{F}_{\mathrm{BB}} = [\mathbf{F}_{\mathrm{BB},1}, \ldots, \mathbf{F}_{\mathrm{BB},m}, \ldots, \mathbf{F}_{\mathrm{BB},M}]$ and $\mathbf{n}_m \in \mathbb{C}^{N_{\mathrm{r}} \times 1}$ are independent and identically distributed (i.i.d) complex additive white Gaussian noise (AWGN) process with distribution $\mathcal{CN}(\mathbf{0}, \sigma^2 \mathbf{I})$.

The received signal $\widetilde{\mathbf{y}}_m \in \mathbb{C}^{N_{\mathrm{s}} \times 1}$ processed at the mth SU is given by

$$\begin{aligned}\widetilde{\mathbf{y}}_m =& \mathbf{W}_{\mathrm{BB},m}^H \mathbf{W}_{\mathrm{RF},m}^H \mathbf{H}_m \mathbf{F}_{\mathrm{RF}} \mathbf{F}_{\mathrm{BB},m} \mathcal{D}(\sqrt{\mathbf{p}_m})\mathbf{s}_m \\ &+ \sum_{n=1, n\neq m}^{M} \mathbf{W}_{\mathrm{BB},m}^H \mathbf{W}_{\mathrm{RF},m}^H \mathbf{H}_m \mathbf{F}_{\mathrm{RF}} \mathbf{F}_{\mathrm{BB},n} \mathcal{D}(\sqrt{\mathbf{p}_n})\mathbf{s}_n \\ &+ \mathbf{W}_{\mathrm{BB},m}^H \mathbf{W}_{\mathrm{RF},m}^H \mathbf{n}_m,\end{aligned} \tag{2}$$

where each SU processes the received signal $\mathbf{y}_m$ by an RF RC $\mathbf{W}_{\mathrm{RF},m} \in \mathbb{C}^{N_{\mathrm{r}} \times M_{\mathrm{r}}}$ followed by the BB RC $\mathbf{W}_{\mathrm{BB},m} \in \mathbb{C}^{M_{\mathrm{r}} \times N_{\mathrm{s}}}$. This treatise considers a fully connected hybrid MIMO architecture, where each RF chain is connected to all the antenna elements via analog phase shifters. Hence, the magnitudes of all elements of $\mathbf{F}_{\mathrm{RF}}$ and $\mathbf{W}_{\mathrm{RF},m}$ are constrained to $\frac{1}{\sqrt{N_{\mathrm{t}}}}$ and $\frac{1}{\sqrt{N_{\mathrm{r}}}}$, respectively.

B. mmWave MIMO channel model

The narrowband mmWave MIMO channel between the mth SU and the CBS, as per the geometrical channel model of [3],

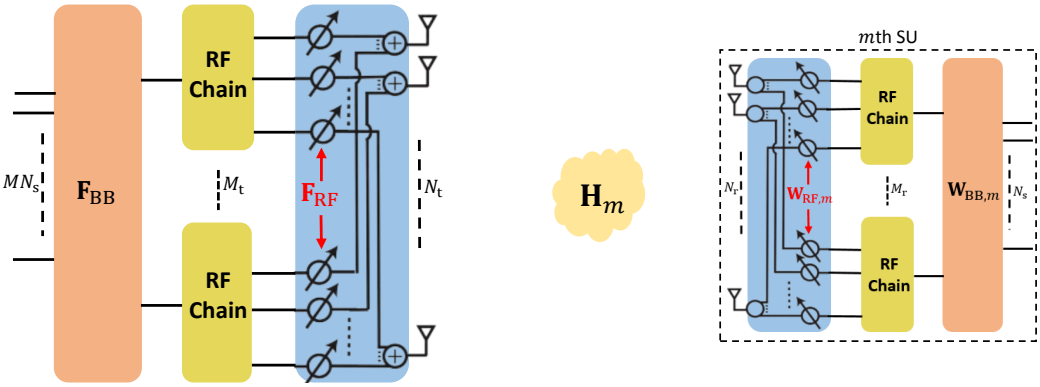

Figure 2: Hybrid transceiver architecture of the CBS and the mth SU in a downlink MU mmWave MIMO CR system.

[5], [7] can be expressed as

$$\mathbf{H}_m = \sqrt{\frac{N_{\mathrm{t}}N_{\mathrm{r}}}{N_p}} \sum_{l=1}^{N_p} \alpha_{m,l}\mathbf{a}_{\mathrm{r}}(\theta_{m,l})\mathbf{a}_{\mathrm{t}}^H(\phi_{m,l}), \tag{3}$$

where $\alpha_{m,l}$ represents the complex-valued multipath gain of the lth path component for the mth SU and N_p denotes the number of scatterers. The quantity $\mathbf{a}_{\mathrm{r}}(\theta_{m,l}) \in \mathbb{C}^{N_{\mathrm{r}}\times 1}$ denotes the antenna array steering vector at the mth SU corresponding to the angle of arrival (AoA) $\theta_{m,l}$ and $\mathbf{a}_{\mathrm{t}}(\phi_{m,l}) \in \mathbb{C}^{N_{\mathrm{t}}\times 1}$ represents the same at the CBS for the angle of departure (AoD) $\phi_{m,l}$. Furthermore, the CBS and each SU are assumed to have uniform linear antenna arrays (ULA), for which their array steering vectors are given by

$$\begin{aligned}
\mathbf{a}_t(\phi_{m,l}) &= \frac{1}{\sqrt{N_{\mathrm{t}}}}[1, e^{j\frac{2\pi d_t \sin(\phi_{m,l})}{\lambda}}, \ldots, e^{j\frac{2\pi(N_{\mathrm{t}}-1)d_t \sin(\phi_{m,l})}{\lambda}}]^T, \\
\mathbf{a}_{\mathrm{r}}(\theta_{m,l}) &= \frac{1}{\sqrt{N_{\mathrm{r}}}}[1, e^{j\frac{2\pi d_r \sin(\theta_{m,l})}{\lambda}}, \ldots, e^{j\frac{2\pi(N_{\mathrm{r}}-1)d_r \sin(\theta_{m,l})}{\lambda}}]^T,
\end{aligned} \tag{4}$$

where d_t and d_r represent the antenna separation at the CBS and each SU, respectively, while λ denotes the wavelength of the mmWave signal.

C. Problem formulation

The objective of this work is to design the hybrid RCs $\{\mathbf{W}_{\mathrm{RF},m}, \mathbf{W}_{\mathrm{BB},m}\}_{m=1}^M$, hybrid TPC $\mathbf{F}_{\mathrm{RF}}, \mathbf{F}_{\mathrm{BB}}$, and the optimal power allocation vector $\mathbf{p}$ for ensuring that the overall SE of the system is maximized, subject to total CBS transmit power constraint i.e., $\|\mathbf{F}_{\mathrm{RF}}\mathbf{F}_{\mathrm{BB}}\mathcal{D}(\sqrt{\mathbf{p}})\|_F^2 \leq P_{\max}$ and a constraint on the interference generated to the PU does not exceed a certain interference threshold I_{th}. Employing the received signal of (2), the SE of the system is expressed as

$$\mathcal{R}_{\mathrm{sum}} = \sum_{m=1}^{M} \log_2\left(|\mathbf{I}_{N_{\mathrm{s}}} + \mathbf{\Gamma}_m|\right), \tag{5}$$

where the matrix $\mathbf{\Gamma}_m \in \mathbb{C}^{N_{\mathrm{s}}\times N_{\mathrm{s}}}$ is given by Eq. (7).Assuming that the CBS has complete knowledge of the channel matrix $\mathbf{G}$, the cumulative interference imposed at the PU because of the downlink communication between the CBS and SUs is expressed as [27]

$$I_{\mathrm{PU}} = \sum_{m=1}^{M} ||\mathbf{G}\mathbf{F}_{\mathrm{RF}}\mathbf{F}_{\mathrm{BB},m}\mathcal{D}(\sqrt{\mathbf{p}_m})||_F^2 . \tag{6}$$

Therefore, the SE maximization problem can be formulated as

$$\begin{aligned}
&\max_{\{\mathbf{W}_{\mathrm{RF},m},\mathbf{W}_{\mathrm{BB},m}\}_{m=1}^M,\mathbf{F}_{\mathrm{RF}},\mathbf{F}_{\mathrm{BB}},\mathcal{D}(\mathbf{p})} \quad \mathcal{R}_{\mathrm{sum}} \\
&\text{s.t.} \begin{cases} |\mathbf{F}_{\mathrm{RF}}(i,j)| = \frac{1}{\sqrt{N_{\mathrm{t}}}}, \forall i,j, \\ |\mathbf{W}_{\mathrm{RF},m}(i,j)| = \frac{1}{\sqrt{N_{\mathrm{r}}}}, \forall i,j,m, \\ I_{\mathrm{PU}} \leq I_{\mathrm{th}}, \\ \|\mathbf{F}_{\mathrm{RF}}\mathbf{F}_{\mathrm{BB}}\mathcal{D}(\sqrt{\mathbf{p}})\|_F^2 \leq P_{\max}, \end{cases}
\end{aligned} \tag{8}$$

where the second last constraint in the above optimization problem limits the interference received at the PU to I_{th}. It can be readily observed that the direct maximization of (8) requires a joint optimization over the five matrix variables $\left(\{\mathbf{W}_{\mathrm{RF},m}, \mathbf{W}_{\mathrm{BB},m}\}_{m=1}^M, \mathbf{F}_{\mathrm{RF}}, \mathbf{F}_{\mathrm{BB}}, \mathcal{D}(\mathbf{p})\right)$. Moreover, solving the global optimization problem is intractable due to the non-convex objective function and non-convex constraints imposed on the elements of the RF RC $\mathbf{W}_{\mathrm{RF},m}$ and TPC $\mathbf{F}_{\mathrm{RF}}$. As a result, we decouple the problem (8) into two sub-optimization problems as follows. In the first step, each SU designs its blind MMSE hybrid RC $\mathbf{W}_{\mathrm{RF},m}, \mathbf{W}_{\mathrm{BB},m}, \forall m$, assuming that the optimal fully digital TPC is being used at the CBS and also considering equal-power allocation for each stream, which is calculated based on the maximum interference level I_{th} tolerated by the PU. In the second step, given the knowledge of the hybrid RCs of each SU, the CBS now designs the TPCs $\mathbf{F}_{\mathrm{RF}}, \mathbf{F}_{\mathrm{BB}}$, and subsequently also determines the optimal power allocation vector $\mathbf{p}$. These steps are now described in detail in the following subsections using the supporting mathematical framework.

III. Blind MMSE Combiner Design at Each SU

In the CR downlink, each SU estimates its own channel to design the appropriate RC without knowing TPC at CBS and then feeds back both the CSI and RC matrices to the CBS for TPC design toward downlink communication. Therefore, we begin by designing the blind hybrid MMSE

$$\mathbf{\Gamma}_m = \frac{\mathbf{W}_{\mathrm{BB},m}^H \mathbf{W}_{\mathrm{RF},m}^H \mathbf{H}_m \mathbf{F}_{\mathrm{RF}} \mathbf{F}_{\mathrm{BB},m} \mathcal{D}(\mathbf{p}_m) \mathbf{F}_{\mathrm{BB},m}^H \mathbf{F}_{\mathrm{RF},m}^H \mathbf{H}_m^H \mathbf{W}_{\mathrm{RF}} \mathbf{W}_{\mathrm{BB},m}}{\sum_{n=1,n\neq m}^{M} \mathbf{W}_{\mathrm{BB},m}^H \mathbf{W}_{\mathrm{RF},m}^H \mathbf{H}_m \mathbf{F}_{\mathrm{RF}} \mathbf{F}_{\mathrm{BB},n} \mathcal{D}(\mathbf{p}_n) \mathbf{F}_{\mathrm{BB},n}^H \mathbf{F}_{\mathrm{RF}}^H \mathbf{H}_m^H \mathbf{W}_{\mathrm{RF},m} \mathbf{W}_{\mathrm{BB},m} + \sigma^2 \mathbf{W}_{\mathrm{BB},m}^H \mathbf{W}_{\mathrm{RF},m}^H \mathbf{W}_{\mathrm{RF},m} \mathbf{W}_{\mathrm{BB},m}} \tag{7}$$

RC comprised of $\mathbf{W}_{\mathrm{RF},m}, \mathbf{W}_{\mathrm{BB},m}$, while assuming the TPC at the CBS to be the optimal unconstrained TPC $\bar{\mathbf{F}}_m^{\mathrm{opt}} = [\bar{\mathbf{F}}_1, \bar{\mathbf{F}}_2, \ldots, \bar{\mathbf{F}}_m, \ldots, \bar{\mathbf{F}}_M] \in \mathbb{C}^{N_{\mathrm{t}} \times M N_{\mathrm{s}}}$ for the mth SU with equal-power allocation to all the streams. Note that the equal-power allocation is based on the fact that the SUs have no information about the channel matrix $\mathbf{G}$ between CBS and PU. Further, to mitigate the MUI at the mth SU, we set $\mathbf{H}_m \bar{\mathbf{F}}_n = 0$ i.e., $\bar{\mathbf{F}}_n \in \mathcal{N}(\mathbf{H}_m), \forall n \neq m$, which can be designed using the SVD of $\mathbf{H}_m = \mathbf{U}_m \mathbf{\Sigma}_m \mathbf{V}_m^H$. Toward this, let us write the SVD of $\mathbf{H}_m$ as

$$\mathbf{H}_m = \begin{bmatrix} \mathbf{U}_m^1 & \mathbf{U}_m^2 \end{bmatrix} \begin{bmatrix} \mathbf{\Sigma}_m^1 & 0 \\ 0 & \mathbf{\Sigma}_m^2 \end{bmatrix} \begin{bmatrix} \mathbf{V}_m^1 & \mathbf{V}_m^2 \end{bmatrix}^H, \tag{9}$$

where $\mathbf{U}_m^1$ comprises the first N_{s} columns of $\mathbf{U}_m$, $\mathbf{\Sigma}_m^1$ consists of the first N_s singular values, and $\mathbf{V}_m^1$ is comprised of the first N_{s} columns of $\mathbf{V}_m$. Hence, the optimal TPC at the mth SU, which eliminates both the ISI and MUI is given by setting, $\bar{\mathbf{F}}_m = \mathbf{V}_m^1$ and $\bar{\mathbf{F}}_{i,i\neq m} = \mathbf{V}_m^2(:, N_t - N_s : N_s)$. Hence, the RCs $\mathbf{W}_{\mathrm{RF},m}, \mathbf{W}_{\mathrm{BB},m}$ are designed for minimizing the mean-squared-error (MSE) between the transmitted and the corresponding processed received signal for each SU. The signal $\bar{\mathbf{y}}_m \in \mathbb{C}^{N_{\mathrm{r}} \times 1}$ received at the mth SU upon assuming $\bar{\mathbf{F}}_m^{\mathrm{opt}}$ at the CBS can be written as

$$\bar{\mathbf{y}}_m = \mathbf{H}_m \bar{\mathbf{F}}_m^{\mathrm{opt}} \mathcal{D}(\sqrt{\mathbf{p}}) \mathbf{s} + \mathbf{n}_m. \tag{10}$$

Furthermore, the blind power allocation ρ_m apportioned for each stream of the mth SU can be calculated by sharing the tolerable interference I_{th} equally amongst the MN_{s} data streams, which is given by $\rho_m = \frac{I_{\mathrm{th}}}{||\mathbf{G}\bar{\mathbf{F}}_m^{\mathrm{opt}}||_F^2}$. With the aid of $\bar{\mathbf{F}}_m^{\mathrm{opt}}$, (10) can be rewritten as

$$\bar{\mathbf{y}}_m = \sqrt{\rho_m} \mathbf{H}_m \bar{\mathbf{F}}_m \mathbf{s}_m + \mathbf{n}_m. \tag{11}$$

Using $\bar{\mathbf{F}}_m = \mathbf{V}_m^1$, Eq. (11) can be approximated as

$$\bar{\mathbf{y}}_m \approx \sqrt{\rho_m} \mathbf{U}_m^1 \mathbf{\Sigma}_m^1 \mathbf{s}_m + \mathbf{n}_m. \tag{12}$$

The hybrid MMSE RC design problem at the mth SU can therefore be formulated as

$$\begin{aligned} &(\mathbf{W}_{\mathrm{RF},m}^{\mathrm{opt}}, \mathbf{W}_{\mathrm{BB},m}^{\mathrm{opt}}) = \\ &\underset{\mathbf{W}_{\mathrm{RF},m}, \mathbf{W}_{\mathrm{BB},m}}{\arg\min} \quad \mathbb{E}\big[||\mathbf{s}_m - \mathbf{W}_{\mathrm{BB},m}^H \mathbf{W}_{\mathrm{RF},m}^H \bar{\mathbf{y}}_m||_2^2\big], \\ &\text{s.t. } |\mathbf{W}_{\mathrm{RF},m}(i,j)| = \frac{1}{\sqrt{N_{\mathrm{r}}}}, \forall i,j, \end{aligned} \tag{13}$$

where one can readily observe that the objective is to minimize the MSE between the transmitted signal $\mathbf{s}_m$ and the processed received signal $\mathbf{W}_{\mathrm{BB},m}^H \mathbf{W}_{\mathrm{RF},m}^H \bar{\mathbf{y}}_m$. It is worth noting that in the absence of the constant magnitude constraints on the elements of $\mathbf{W}_{\mathrm{RF},m}$, the fully digital solution of (13) is given by the linear MMSE RC $\mathbf{W}_{\mathrm{MMSE},m}^H$ as [33]

$$\mathbf{W}_{\mathrm{MMSE},m}^H = \mathbf{R}_{s\bar{\mathrm{y}},m} \mathbf{R}_{\bar{\mathrm{y}}\bar{\mathrm{y}},m}^{-1}. \tag{14}$$

Using the received signal $\bar{\mathbf{y}}_m$ and $\mathbf{s}_m$, one can derive the covariance matrices as follows

$$\begin{aligned} &\mathbf{R}_{\mathrm{s}\bar{\mathrm{y}},m} = \mathbb{E}[\mathbf{s}_m \bar{\mathbf{y}}_m^H] = \sqrt{\rho_m} \mathbf{\Sigma}_m^1 \mathbf{U}_m^{1^H}, \\ &\mathbf{R}_{\bar{\mathrm{y}}\bar{\mathrm{y}},m} = \mathbb{E}[\bar{\mathbf{y}}_m \bar{\mathbf{y}}_m^H] = \mathbf{U}_m^1 \underbrace{(\rho_m (\mathbf{\Sigma}_m^1)^2 + \sigma^2 \mathbf{I}_{N_{\mathrm{s}}})}_{\mathbf{\Lambda}_m} (\mathbf{U}_m^1)^H. \end{aligned} \tag{15}$$

The linear MMSE RC $\mathbf{W}_{\mathrm{MMSE},m}$ using (15) is given by

$$\begin{aligned} \mathbf{W}_{\mathrm{MMSE},m}^H &= \mathbf{R}_{\mathrm{s}\bar{\mathrm{y}},m} \mathbf{R}_{\bar{\mathrm{y}}\bar{\mathrm{y}},m}^{-1} \\ &= \sqrt{\rho_m} \mathbf{\Sigma}_m^1 (\mathbf{U}_m^1)^H \left(\mathbf{U}_m^1 \mathbf{\Lambda}_m (\mathbf{U}_m^1)^H \right)^{-1}. \end{aligned} \tag{16}$$

By exploiting the fact that if $\mathbf{A}, \mathbf{B}$ and $\mathbf{C}$ are invertible, $(\mathbf{ABC})^{-1} = \mathbf{C}^{-1}\mathbf{B}^{-1}\mathbf{A}^{-1}$ and $(\mathbf{U}_m^1)^{-1} = (\mathbf{U}_m^1)^H$, we have

$$\begin{aligned} \mathbf{W}_{\mathrm{MMSE},m}^H &= \sqrt{\rho_m} \mathbf{\Sigma}_m^1 \underbrace{(\mathbf{U}_m^1)^H \mathbf{U}_m^1}_{\mathbf{I}_{N_{\mathrm{s}}}} \mathbf{\Lambda}_m^{-1} (\mathbf{U}_m^1)^H \\ &= \sqrt{\rho_m} \mathbf{\Sigma}_m^1 \mathbf{\Lambda}_m^{-1} (\mathbf{U}_m^1)^H \\ &= \sqrt{\rho_m} \mathbf{\Sigma}_m^1 (\rho_m (\mathbf{\Sigma}_m^1)^2 + \sigma^2 \mathbf{I}_{N_{\mathrm{s}}})^{-1} (\mathbf{U}_m^1)^H \\ &= \frac{1}{\sqrt{\rho_m}} (\mathbf{\Sigma}_m^1) \left((\mathbf{\Sigma}_m^1)^2 + \frac{\sigma^2}{\rho_m} \mathbf{I}_{N_{\mathrm{s}}} \right)^{-1} (\mathbf{U}_m^1)^H \end{aligned} \tag{17}$$

Note that it is easy to compute the above matrix $\mathbf{W}_{\mathrm{MMSE},m}$ at each SU, since the inverse of the diagonal matrix $\left((\mathbf{\Sigma}_m^1)^2 + \frac{\sigma^2}{\rho_m} \mathbf{I}_{N_{\mathrm{s}}} \right)^{-1}$ is easy to determine. Furthermore, the optimization problem (13) can be reformulated as

$$\begin{aligned} &(\mathbf{W}_{\mathrm{RF},m}^{\mathrm{opt}}, \mathbf{W}_{\mathrm{BB},m}^{\mathrm{opt}}) = \\ &\underset{\mathbf{W}_{\mathrm{RF},m}, \mathbf{W}_{\mathrm{BB},m}}{\arg\min} \left|\left| \mathbf{R}_{\bar{\mathrm{y}}\bar{\mathrm{y}},m}^{\frac{1}{2}} (\mathbf{W}_{\mathrm{MMSE},m} - \mathbf{W}_{\mathrm{RF},m} \mathbf{W}_{\mathrm{BB},m}) \right|\right|_F^2, \\ &\text{s.t. } |\mathbf{W}_{\mathrm{RF},m}(i,j)| = \frac{1}{\sqrt{N_{\mathrm{r}}}}, \forall i,j. \end{aligned} \tag{18}$$

However, the non-convex nature of the constraints imposed on the elements of $\mathbf{W}_{\mathrm{RF},m}$ renders the solution of (18) intractable. This problem can be addressed by employing the following key observations:

1) Observe Eq. (17) that the columns of the unitary matrix $\mathbf{U}_m^1$ form an orthonormnal basis for the column space of the matrix $\mathbf{W}_{\mathrm{MMSE},m}$, i.e., $\mathcal{C}(\mathbf{W}_{\mathrm{MMSE},m}) = \mathcal{C}(\mathbf{U}_m^1)$.
2) Exploiting the structure of the mmWave MIMO channel in (3), one can see that the row and column spaces of $\mathbf{H}_m$ are subsets of the transmit and receive array response matrices, $\mathbf{A}_{\mathrm{t},m} \in \mathbb{C}^{N_{\mathrm{t}} \times L_{\mathrm{p}}}$ and $\mathbf{A}_{\mathrm{r},m} \in \mathbb{C}^{N_{\mathrm{r}} \times L_{\mathrm{p}}}$ respectively, i.e., we have $\mathcal{R}(\mathbf{H}_m) = \mathcal{C}(\mathbf{A}_{\mathrm{t},m}^H)$ and $\mathcal{C}(\mathbf{H}_m) = \mathcal{C}(\mathbf{A}_{\mathrm{r},m})$, where $\mathbf{A}_{\mathrm{t},m} = [\mathbf{a}_{\mathrm{t}}(\phi_{m,1}), \ldots, \mathbf{a}_{\mathrm{t}}(\phi_{m,L_p})]$ and $\mathbf{A}_{\mathrm{r},m} = [\mathbf{a}_{\mathrm{r}}(\theta_{m,1}), \ldots, \mathbf{a}_{\mathrm{r}}(\theta_{m,L_p})]$. Furthermore, it follows from (9) that $\mathcal{C}(\mathbf{U}_m^1) \subseteq \mathcal{C}(\mathbf{H}_m) = \mathcal{C}(\mathbf{A}_{\mathrm{r},m})$, which finally implies that $\mathcal{C}(\mathbf{W}_{\mathrm{MMSE},m}) \subseteq \mathcal{C}(\mathbf{A}_{\mathrm{r},m})$.
3) Furthermore, recall that the elements of the RF RC $\mathbf{W}_{\mathrm{RF},m}$ are constant gain phase quantities. Hence, the

columns of $\mathbf{W}_{\mathrm{RF},m}$ can be suitably selected from the columns of $\mathbf{A}_{\mathrm{r},m}$. Therefore, the pertinent RC design problem reduces to selecting a suitable set of M_{r} columns from the receiver array response matrix $\mathbf{A}_{\mathrm{r},m}$ followed by determining the optimal BB RC.

As a result, the constraint on $\mathbf{W}_{\mathrm{RF},m}$ can be readily integrated into the optimization problem of (18), which yields the following updated problem

$$\begin{aligned}&\widetilde{\mathbf{W}}_{\mathrm{BB},m}^{\mathrm{opt}} = \\ &\underset{\widetilde{\mathbf{W}}_{\mathrm{BB},m}}{\arg\min} \left|\left|\mathbf{R}_{\bar{\mathrm{y}}\bar{\mathrm{y}},m}^{\frac{1}{2}}(\mathbf{W}_{\mathrm{MMSE},m} - \mathbf{A}_{\mathrm{r},m}\widetilde{\mathbf{W}}_{\mathrm{BB},m})\right|\right|_F^2, \\ &\text{s.t. } \left|\left|\mathrm{diag}\left(\widetilde{\mathbf{W}}_{\mathrm{BB},m}\widetilde{\mathbf{W}}_{\mathrm{BB},m}^H\right)\right|\right|_0 = M_{\mathrm{r}},\end{aligned} \tag{19}$$

where $\widetilde{\mathbf{W}}_{\mathrm{BB},m} \in \mathbb{C}^{L_{\mathrm{p}}\times N_{\mathrm{s}}}$ denotes the intermediate BB RC matrix, whose M_{r} non-zero rows form the desired BB RC $\mathbf{W}_{\mathrm{BB},m}$. The constraint in (19) states that the matrix $\widetilde{\mathbf{W}}_{\mathrm{BB},m}$ cannot have more than M_{r} non-zero rows, leading to its simultaneous sparse structure. Furthermore, $\mathbf{W}_{\mathrm{RF},m}$ can be obtained by extracting the columns of $\mathbf{A}_{\mathrm{r},m}$, whose indices correspond to the non-zero rows of $\widetilde{\mathbf{W}}_{\mathrm{BB},m}$. An important observation in (19) is that one has to have perfect knowledge of the AoAs to construct the matrix $\mathbf{A}_{\mathrm{r},m}$, which is practically difficult to obtain. Toward this end, we consider a discrete fourier transform (DFT) codebook $\mathbf{G}_{\mathrm{Rx}} \in \mathbb{C}^{N_{\mathrm{r}}\times N_{\mathrm{r}}}$ known at each receiver, which contains the vectors $\mathbf{a}(\xi_m) \in \mathbb{C}^{N_{\mathrm{r}}\times 1}$ defined as

$$\mathbf{a}(\xi_m) = \frac{1}{\sqrt{N_{\mathrm{r}}}}[1, e^{j\xi_m}, \ldots, e^{j(N_{\mathrm{r}}-1)\xi_m}]^T, \tag{20}$$

where the angle ξ_m is given by

$$\xi_m = \frac{2\pi(m-1)}{N_{\mathrm{r}}}, m = 1, \ldots, N_{\mathrm{r}}. \tag{21}$$

Hence, our codebook $\mathbf{G}_{\mathrm{Rx}}$ contains the set of DFT-basis vectors as

$$\mathbf{G}_{\mathrm{Rx}} = \{\mathbf{a}(\xi_1), \mathbf{a}(\xi_2), \ldots, \mathbf{a}(\xi_{N_{\mathrm{r}}})\}. \tag{22}$$

Employing this, the equivalent hybrid RC design problem can be reformulated as

$$\begin{aligned}&\overline{\mathbf{W}}_{\mathrm{BB},m}^{\mathrm{opt}} = \\ &\underset{\overline{\mathbf{W}}_{\mathrm{BB},m}}{\arg\min} \left|\left|\mathbf{R}_{\bar{\mathrm{y}}\bar{\mathrm{y}},m}^{\frac{1}{2}}(\mathbf{W}_{\mathrm{MMSE},m} - \mathbf{G}_{\mathrm{Rx}}\overline{\mathbf{W}}_{\mathrm{BB},m})\right|\right|_F^2, \\ &\text{s.t. } \left|\left|\mathrm{diag}(\overline{\mathbf{W}}_{\mathrm{BB},m}\overline{\mathbf{W}}_{\mathrm{BB},m}^H)\right|\right|_0 = M_{\mathrm{r}}.\end{aligned} \tag{23}$$

The solution of the optimization problem above can be obtained using the SOMP-based simultaneous sparse signal recovery technique. The key steps of the SOMP technique are given in Algorithm 1. In each iteration, step-4 and step-5 find the index q of the column of the codebook $\mathbf{G}_{\mathrm{Rx}}$, which has the maximum weighted projection along the residue $\mathbf{W}_{\mathrm{res},m}$ determined in the previous iteration. Step-6 updates the matrix $\mathbf{W}_{\mathrm{RF},m}$ by including the qth column of $\mathbf{G}_{\mathrm{Rx}}$. Step-7 and step-8 compute the BB RC $\mathbf{W}_{\mathrm{BB},m}$ using the weighted least squares solution and the corresponding residue matrix $\mathbf{W}_{\mathrm{res},m}$, respectively. The algorithm concludes when the number of columns in $\mathbf{W}_{\mathrm{RF},m}$ equals M_{r}, at which point the algorithm terminates and returns the matrices $\mathbf{W}_{\mathrm{RF},m}, \mathbf{W}_{\mathrm{BB},m}$. The computational complexity of the blind MMSE combiner algorithm can be explicitly evaluated as follows. The complexity of Step-1 in Algorithm 1 that evaluates the MMSE RC $\mathbf{W}_{\mathrm{MMSE}}$ using (17) is of the order $\mathcal{O}(N_{\mathrm{r}}N_{\mathrm{s}}^3)$ since it involves the inversion of a diagonal matrix followed by matrix multiplication. Furthermore, the worst-case complexity of the iterative loop from Step-3 to Step-9 corresponds to Step 4, that has a complexity of $\mathcal{O}(N_{\mathrm{r}}^2 M_{\mathrm{r}} N_{\mathrm{s}})$ [4]. Therefore, the overall complexity of the proposed blind MMSE RC is $\mathcal{O}(N_{\mathrm{r}}^2 M_{\mathrm{r}} N_{\mathrm{s}})$.

Finally, each SU feeds back its hybrid RC to the CBS for hybrid TPC design and optimal power allocation. This procedure is discussed in the subsequent section in detail.

Algorithm 1 Blind MMSE combining based on SOMP at the mth SU

Require: $\mathbf{W}_{\mathrm{MMSE},m}$
1: $\mathbf{W}_{\mathrm{RF},m} =$ Empty Matrix
2: $\mathbf{W}_{\mathrm{res},m} = \mathbf{W}_{\mathrm{MMSE},m}$
3: **for** $i \leq M_{\mathrm{r}}$ **do**
4: $\quad \mathbf{\Psi} = \mathbf{G}_{\mathrm{Rx}}^H \mathbf{R}_{\bar{\mathrm{y}}\bar{\mathrm{y}},m} \mathbf{W}_{\mathrm{res},m}$
5: $\quad q = \arg\max_{l=1,\ldots G_r} (\mathbf{\Psi}\mathbf{\Psi}^H)_{l,l}$
6: $\quad \mathbf{W}_{\mathrm{RF},m} = [\mathbf{W}_{\mathrm{RF},m} | \mathbf{G}_{\mathrm{Rx}}^{(q)}]$
7: $\quad \mathbf{W}_{\mathrm{BB},m} = (\mathbf{W}_{\mathrm{RF},m}^H \mathbf{R}_{\bar{\mathrm{y}}\bar{\mathrm{y}},m} \mathbf{W}_{\mathrm{RF},m})^{-1} \mathbf{W}_{\mathrm{RF},m}^H \times \mathbf{R}_{\bar{\mathrm{y}}\bar{\mathrm{y}},m} \mathbf{W}_{\mathrm{MMSE},m}$
8: $\quad \mathbf{W}_{\mathrm{res},m} = \frac{\mathbf{W}_{\mathrm{MMSE},m} - \mathbf{W}_{\mathrm{RF},m}\mathbf{W}_{\mathrm{BB},m}}{||\mathbf{W}_{\mathrm{MMSE},m} - \mathbf{W}_{\mathrm{RF},m}\mathbf{W}_{\mathrm{BB},m}||_{\mathbf{F}}}$
9: **end for**
10: **return** $\mathbf{W}_{\mathrm{RF},m}, \mathbf{W}_{\mathrm{BB},m}$

IV. HYBRID PRECODER DESIGN AND OPTIMAL POWER ALLOCATION AT CBS

Given the knowledge of the hybrid RCs fed back from all the SUs, the CBS designs the hybrid TPC $\mathbf{F}_{\mathrm{RF}}, \mathbf{F}_{\mathrm{BB}}$ and determines the optimal power allocation vector $\mathbf{p}$ on the basis of the maximum tolerable interference I_{th} and total transmit power $P_{\max}$ at the CBS, which maximizes the overall system SE given by Eq. (5), as follows. Let the SU's effective channel matrix be defined as $\widetilde{\mathbf{H}}_m = \mathbf{W}_{\mathrm{BB},m}^H \mathbf{W}_{\mathrm{RF},m}^H \mathbf{H}_m \in \mathbb{C}^{N_{\mathrm{s}}\times N_{\mathrm{t}}}, \forall m$. Therefore, the TPC optimization problem can be formulated as

$$\begin{aligned}&\max_{\mathbf{F}_{\mathrm{RF}}, \mathbf{F}_{\mathrm{BB}}, \mathcal{D}(\mathbf{p})} \mathcal{R}_{\mathrm{sum}} \\ &\text{s.t.} \begin{cases} |\mathbf{F}_{\mathrm{RF}}(i,j)| = \frac{1}{\sqrt{N_{\mathrm{t}}}}, \forall i,j, \\ I_{\mathrm{PU}} \leq I_{\mathrm{th}}, \\ \|\mathbf{F}_{\mathrm{RF}}\mathbf{F}_{\mathrm{BB}}\mathcal{D}(\sqrt{\mathbf{p}})\|_F^2 \leq P_{\max}. \end{cases}\end{aligned} \tag{24}$$

Recall that the analog TPC $\mathbf{F}_{\mathrm{RF}}$ is the same for all SUs, whereas the overall BB TPC obeys $\mathbf{F}_{\mathrm{BB}} = [\mathbf{F}_{\mathrm{BB},1}, \ldots, \mathbf{F}_{\mathrm{BB},m}, \ldots, \mathbf{F}_{\mathrm{BB},M}]$, where $\mathbf{F}_{\mathrm{BB},m}$ corresponds to the BB TPC of the mth SU. To maximize the SE in (24),

we now decompose the BB TPC of the mth SU into two sub-matrices $\mathbf{F}^1_{\mathrm{BB},m}$ and $\mathbf{F}^2_{\mathrm{BB},m}$. As a result, the design of the TPC is divided into two stages. In stage-1, the RF TPC $\mathbf{F}_{\mathrm{RF}}$ and BB TPC $\mathbf{F}^1_{\mathrm{BB}} = [\mathbf{F}^1_{\mathrm{BB},1}, \ldots, \mathbf{F}^1_{\mathrm{BB},m}, \ldots, \mathbf{F}^1_{\mathrm{BB},M}] \in \mathbb{C}^{M_{\mathrm{t}} \times MN_{\mathrm{s}}}$ are designed jointly for maximizing each SU's SE, while ignoring the MUI. In stage-2, the BB TPC $\mathbf{F}^2_{\mathrm{BB}} = [\mathbf{F}^2_{\mathrm{BB},1}, \ldots, \mathbf{F}^2_{\mathrm{BB},m}, \ldots, \mathbf{F}^2_{\mathrm{BB},M}] \in \mathbb{C}^{N_{\mathrm{s}} \times MN_{\mathrm{s}}}$ is constructed for mitigating the MUI. The design steps for both these stages are described below in detail.

Note that ignoring the MUI, the SE of the mth SU is given by

$$\mathcal{R}_m = \log_2 \Big(\Big| \mathbf{I}_{N_{\mathrm{s}}} + \mathbf{R}^{-1}_{\mathrm{nn},m} \widetilde{\mathbf{H}}_m \mathbf{F}_{\mathrm{RF}} \mathbf{F}^1_{\mathrm{BB},m} \mathbf{F}^2_{\mathrm{BB},m} \mathcal{D}(\mathbf{p}_m) (\mathbf{F}^2_{\mathrm{BB},m})^H (\mathbf{F}^1_{\mathrm{BB},m})^H \mathbf{F}^H_{\mathrm{RF}} \widetilde{\mathbf{H}}^H_m \Big| \Big), \tag{25}$$

where $\mathbf{R}_{\mathrm{nn},m} = \sigma^2 \mathbf{W}^H_{\mathrm{BB},m} \mathbf{W}^H_{\mathrm{RF},m} \mathbf{W}_{\mathrm{RF},m} \mathbf{W}_{\mathrm{BB},m}$ represents the covariance of the combined noise. Furthermore, using the SVD of $\widetilde{\mathbf{H}}_m$ as $\widetilde{\mathbf{H}}_m = \widetilde{\mathbf{U}}_m \widetilde{\mathbf{\Sigma}}_m \widetilde{\mathbf{V}}^H_m$ and following the steps given in Appendix A, one can closely approximate $\mathcal{R}_m$ as

$$\begin{aligned} \mathcal{R}_m \approx & \log_2 \Big(\Big| \mathbf{I}_{N_{\mathrm{s}}} \\ & + (\mathbf{F}^2_{\mathrm{BB},m})^H (\widetilde{\mathbf{\Sigma}}^1_m)^H \widetilde{\mathbf{U}}^H_m \mathbf{R}^{-1}_{\mathrm{nn},m} \widetilde{\mathbf{U}}_m \widetilde{\mathbf{\Sigma}}^1_m \mathbf{F}^2_{\mathrm{BB},m} \mathcal{D}(\mathbf{p}_m) \Big| \Big) \\ & - \Big(N_{\mathbf{s}} - ||(\widetilde{\mathbf{V}}^1_m)^H \mathbf{F}_{\mathrm{RF}} \mathbf{F}^1_{\mathrm{BB},m}||^2_F \Big), \end{aligned} \tag{26}$$

where $\widetilde{\mathbf{\Sigma}}^1_m \in \mathbb{C}^{N_{\mathrm{s}} \times N_{\mathrm{s}}}$ and $\widetilde{\mathbf{V}}^1_m \in \mathbb{C}^{N_{\mathrm{t}} \times N_{\mathrm{s}}}$ denote the first N_{s} columns of the matrices $\widetilde{\mathbf{\Sigma}}_m$ and $\widetilde{\mathbf{V}}_m$, respectively. Note that the power allocation vector $\mathbf{p}_m$ and hybrid TPC $\mathbf{F}_{\mathrm{RF}}, \mathbf{F}^1_{\mathrm{BB},m}$ are encapsulated in the first and second terms of $\mathcal{R}_m$, respectively, which divides the TPC optimization problem of (25) into two sub-optimization problems. We formulate the first sub-optimization problem to design the hybrid TPC under hardware constraints, which is solved using a two-stage procedure. The second sub-optimization problem constructed for power allocation incorporates the transmit power and interference threshold constraints. Then a closed-form solution is derived for it. Both these sub-optimization problems and their solutions are discussed in the subsequent subsections.

A. Hybrid TPC design

One can observe that, when the term $\mathbf{F}_{\mathrm{RF}} \mathbf{F}^1_{\mathrm{BB},m}$ is set as a unitary matrix, the second term in (26) reduces to the squared chordal distance between the two points, namely, the optimal unconstrained TPC for the mth SU $\mathbf{F}^{\mathrm{opt}}_m = \widetilde{\mathbf{V}}^1_m$ and $\mathbf{F}_{\mathrm{RF}} \mathbf{F}^1_{\mathrm{BB},m}$ on the Grassmann manifold. Using the approximation $(\widetilde{\mathbf{V}}^1_m)^H \mathbf{F}_{\mathrm{RF}} \mathbf{F}^1_{\mathrm{BB},m} \approx \mathbf{I}_{N_{\mathrm{s}}}$ from Appendix A and exploiting the manifold's locally Euclidean property, one can replace the chordal distance by the Euclidean distance $||\mathbf{F}^{\mathrm{opt}}_m - \mathbf{F}_{\mathrm{RF}} \mathbf{F}^1_{\mathrm{BB},m}||_F$. Moreover, since the MUI has been ignored in the first stage, the overall TPC design problem can be decoupled into M single-user TPC design problems. Hence, it can be written as

$$\begin{aligned} \left(\mathbf{F}^{\mathrm{opt}}_{\mathrm{RF}}, \mathbf{F}^{1,\mathrm{opt}}_{\mathrm{BB}} \right) &= \arg \min_{\mathbf{F}^1_{\mathrm{BB}}} \left|\left| \mathbf{F}^{\mathrm{opt}} - \mathbf{F}_{\mathrm{RF}} \mathbf{F}^1_{\mathrm{BB}} \right|\right|_F, \\ & \text{s.t. } |\mathbf{F}_{\mathrm{RF}}(i,j)| = \frac{1}{\sqrt{N_{\mathrm{t}}}}, \forall i, j, \end{aligned} \tag{27}$$

where $\mathbf{F}^{\mathrm{opt}} = [\mathbf{F}^{\mathrm{opt}}_1, \ldots, \mathbf{F}^{\mathrm{opt}}_m, \ldots, \mathbf{F}^{\mathrm{opt}}_M] \in \mathbb{C}^{M_{\mathrm{t}} \times MN_{\mathrm{s}}}$ is the stacked optimal unconstrained TPC of all the SUs. Observe that the above TPC design problem closely resembles the design problem of each SU's hybrid RC in (18). This can once again be solved by using the SOMP described in Section III. One can now exploit the properties of the mm Wave MIMO channel as discussed in Section III for obtaining the solution of (27). The corresponding optimization problem can be reformulated as

$$\begin{aligned} \overline{\mathbf{F}}^{1,\mathrm{opt}}_{\mathrm{BB}} &= \arg \min_{\overline{\mathbf{F}}^1_{\mathrm{BB}}} \left|\left| \mathbf{F}^{\mathrm{opt}} - \mathbf{G}_{\mathrm{Tx}} \overline{\mathbf{F}}^1_{\mathrm{BB}} \right|\right|^2_F, \\ & \text{s.t. } \left|\left| \mathrm{diag}(\overline{\mathbf{F}}^1_{\mathrm{BB}} (\overline{\mathbf{F}}^1_{\mathrm{BB}})^H) \right|\right|_0 = M_{\mathrm{t}}. \end{aligned} \tag{28}$$

Here, $\mathbf{G}_{\mathrm{Tx}} \in \mathbb{C}^{N_{\mathrm{t}} \times 2N_{\mathrm{t}}}$ represents an over-complete dictionary, which contains the vectors $\mathbf{b}(\xi_i) \in \mathbb{C}^{N_{\mathrm{t}} \times 1}$, $i = 1, \ldots, 2N_{\mathrm{t}}$, defined as

$$\mathbf{b}(\xi_i) = \frac{1}{\sqrt{N_{\mathrm{t}}}} [1, e^{j\zeta_i}, \ldots, e^{j(N_{\mathrm{t}}-1)\zeta_i}]^T, \tag{29}$$

where the angle ξ_i is given by

$$\xi_i = \frac{\pi(i-1)}{N_{\mathrm{t}}}, i = 1, \ldots, 2N_{\mathrm{t}}. \tag{30}$$

Similarly, the solution to the optimization problem (28) can be obtained using the SOMP-based simultaneous sparse signal recovery technique, as already discussed in Algorithm 1. Furthermore, in order to mitigate the MUI, one has to design the BB TPC $\mathbf{F}^2_{\mathrm{BB}}$ in the second stage. In order to keep the design complexity low, we employ the zero forcing (ZF) technique to determine $\mathbf{F}^2_{\mathrm{BB}}$. As per this approach, the CBS computes the effective channel matrix corresponding to the mth SU as $\widetilde{\mathbf{H}}^{\mathrm{eff}}_m = \widetilde{\mathbf{H}}_m \mathbf{F}_{\mathrm{RF}} \mathbf{F}^1_{\mathrm{BB},m} \in \mathbb{C}^{N_{\mathrm{s}} \times N_{\mathrm{s}}}, \forall m$, and stacks them in a matrix as $\overline{\mathbf{H}} = \left[(\widetilde{\mathbf{H}}^{\mathrm{eff}}_1)^T \ldots (\widetilde{\mathbf{H}}^{\mathrm{eff}}_m)^T \ldots (\widetilde{\mathbf{H}}^{\mathrm{eff}}_M)^T \right]^T \in \mathbb{C}^{MN_{\mathrm{s}} \times N_{\mathrm{s}}}$. Subsequently, the ZF BB precoder $\mathbf{F}_{\mathrm{BB},2}$ is designed as

$$\mathbf{F}^2_{\mathrm{BB}} = \left(\overline{\mathbf{H}}^H \overline{\mathbf{H}} \right)^{-1} \overline{\mathbf{H}}^H \tag{31}$$

Finally, the BB precoder corresponding to the mth SU is given as $\mathbf{F}_{\mathrm{BB},m} = \mathbf{F}^1_{\mathrm{BB},m} \mathbf{F}^2_{\mathrm{BB},m}$. The overall design procedure is summarized in Algorithm2. The optimization problem to determine the power allocation vector $\{\mathbf{p}_m\}_{m=1}^M$ is discussed next.

Algorithm 2 Two stage hybrid precoding at the CBS

Require: $\mathbf{F}^{\mathrm{opt}} = [\mathbf{F}^{\mathrm{opt}}_1, \ldots, \mathbf{F}^{\mathrm{opt}}_M]$

1: Employ SOMP to obtain $\mathbf{F}_{\mathrm{RF}}, \mathbf{F}^1_{\mathrm{BB}}$
2: Design $\mathbf{F}^2_{\mathrm{BB}}$ using equation (31)
3: $\mathbf{F}_{\mathrm{BB},m} = \mathbf{F}^1_{\mathrm{BB},m} \mathbf{F}^2_{\mathrm{BB},m}$
4: **return** $\mathbf{F}_{\mathrm{RF}}, \mathbf{F}_{\mathrm{BB},m}, \forall m$.

B. Sum SE maximization

Using (26), the optimal power allocation for sum SE maximization can be formulated as

$$\begin{aligned}\mathbf{p}^{\text{opt}} = \max_{\{\mathbf{p}_m\}_{m=1}^{M}} & \sum_{m=1}^{M} \log_2 \Big(\Big| \mathbf{I}_{N_\text{s}} \\ & + (\mathbf{F}_{\text{BB},m}^2)^H (\widetilde{\mathbf{\Sigma}}_m^1)^H \widetilde{\mathbf{U}}_m^H \mathbf{R}_{\text{nn},m}^{-1} \widetilde{\mathbf{U}}_m \widetilde{\mathbf{\Sigma}}_m^1 \mathbf{F}_{\text{BB},m}^2 \mathcal{D}(\mathbf{p}_m) \Big| \Big) \\ & \text{s.t. } I_{\text{PU}} \leq I_{\text{th}}, \\ & \|\mathbf{F}_{\text{RF}} \mathbf{F}_{\text{BB}} \mathcal{D}(\sqrt{\mathbf{p}})\|_F^2 \leq P_{\max}. \end{aligned} \tag{32}$$

Let us now define the matrix $\mathbf{\Upsilon}_m \in \mathbb{C}^{N_\text{s} \times N_\text{s}}$ as

$$\begin{aligned}\mathbf{\Upsilon}_m =& (\mathbf{F}_{\text{BB},m}^2)^H (\widetilde{\mathbf{\Sigma}}_m^1)^H \widetilde{\mathbf{U}}_m^H \mathbf{R}_{\text{nn},m}^{-1} \widetilde{\mathbf{U}}_m \widetilde{\mathbf{\Sigma}}_m^1 \mathbf{F}_{\text{BB},m}^2, \\ \overset{a}{\approx} & \frac{1}{\sigma^2} \begin{bmatrix} \gamma_{m,1}^2 \|\mathbf{f}_{\text{BB},m}^{2,(1)}\|^2 & \dots & \mathbf{0} \\ & \ddots & \\ \mathbf{0} & \dots & \gamma_{m,N_\text{s}}^2 \|\mathbf{f}_{\text{BB},m}^{2,(N_\text{s})}\|^2 \end{bmatrix}, \end{aligned} \tag{33}$$

where $\gamma_{m,i}$ represents the ith principal diagonal element of the matrix $\widetilde{\mathbf{\Sigma}}_m^1$ and $\mathbf{f}_{\text{BB},m}^{2,(i)}$ denotes the ith column of $\mathbf{F}_{\text{BB},m}^2$. Furthermore, the approximation (a) employed in (33) follows by noting that $\mathbf{W}_{\text{RF},m}^H \mathbf{W}_{\text{BB},m}^H \mathbf{W}_{\text{BB},m} \mathbf{W}_{\text{RF},m} \approx \mathbf{I}_{N_\text{s}}$ [2], and the columns of $\mathbf{F}_{\text{BB},m}^2$ are orthogonal, especially for large antenna arrays [5]. Now, the interference power constraint at the PU due to the transmission by the CBS can be formulated as

$$\begin{aligned} & I_{\text{PU}} \leq I_{\text{th}}, \\ & \sum_{m=1}^{M} \text{Tr}\left(\mathbf{G}\mathbf{F}_{\text{RF}}\mathbf{F}_{\mathbf{BB},m}\mathcal{D}(\mathbf{p}_m)\mathbf{F}_{\mathbf{BB},m}^H\mathbf{F}_{\text{RF}}^H\mathbf{G}^H\right) \leq I_{\text{th}}, \\ & \sum_{m=1}^{M} \text{Tr}\Big(\mathcal{D}(\mathbf{p}_m) \underbrace{\mathbf{F}_{\mathbf{BB},m}^H\mathbf{F}_{\text{RF}}^H\mathbf{G}^H\mathbf{G}\mathbf{F}_{\text{RF}}\mathbf{F}_{\text{BB},m}}_{\hat{\mathbf{Z}}_m}\Big) \leq I_{\text{th}}, \\ & \sum_{m=1}^{M}\sum_{d=1}^{N_\text{s}} p_{m,d}\zeta_{m,d} \leq I_{\text{th}}, \end{aligned} \tag{34}$$

where $p_{m,d}$ and $\zeta_{m,d}$ are dth diagonal elements of $\mathcal{D}(\mathbf{p}_m)$ and $\hat{\mathbf{Z}}_m$, respectively. Similarly, the total transmit power constraint at CBS can be rewritten as

$$\sum_{m=1}^{M}\sum_{d=1}^{N_\text{s}} p_{m,d}\, t_{m,d} \leq P_{\max}, \tag{35}$$

where $t_{m,d}$ is dth diagonal element of the matrix $\hat{\mathbf{T}}_m = \mathbf{F}_{\mathbf{BB},m}^H\mathbf{F}_{\text{RF}}^H\mathbf{F}_{\text{RF}}\mathbf{F}_{\text{BB},m}$. Therefore, the sum SE maximization for the mmWave MIMO channel based CR system is given by

$$\begin{aligned} \max_{p_{m,d}} \quad & \sum_{m=1}^{M}\sum_{d=1}^{N_\text{s}} \log_2\left(1 + \frac{\gamma_{m,d}^2\|\mathbf{f}_{\text{BB},m}^{2,(d)}\|^2}{\sigma^2} p_{m,d}\right) \\ \text{s.t.} \quad & \sum_{m=1}^{M}\sum_{d=1}^{N_\text{s}} p_{m,d}\zeta_{m,d} \leq I_{\text{th}}, \\ & \sum_{m=1}^{M}\sum_{d=1}^{N_\text{s}} p_{m,d}t_{m,d} \leq P_{\max}, \\ & p_{m,d} \geq 0. \end{aligned} \tag{36}$$

The theorem below obtains the optimal power $p_{m,d}$ allocated to the mth SU and its dth stream.

Theorem 1. *The SE of the system given in* (36) *is maximized by*

$$p_{m,d} = \max\left\{0, \frac{1}{\lambda\zeta_{m,d} + \omega t_{m,d}} - \frac{\sigma^2}{\gamma_{m,d}^2\|\mathbf{f}_{\text{BB},m}^{2,(d)}\|^2}\right\} \forall m, d. \tag{37}$$

Proof. The proof is given in Appendix B. □

C. Maximizing geometric mean of SU rates

The optimal power allocation to maximize the GM of SU rates can be formulated as

$$\begin{aligned} \mathbf{p}^{\text{opt}} = \max_{\{\mathbf{p}_m\}_{m=1}^{M}} & \left(\Pi_{m=1}^{M} R_m(\mathbf{p})\right)^{1/M} \\ & \text{s.t. } I_{\text{PU}} \leq I_{\text{th}} \\ & \|\mathbf{F}_{\text{RF}}\mathbf{F}_{\text{BB}}\mathcal{D}(\sqrt{\mathbf{p}})\|_F^2 \leq P_{\max}. \end{aligned} \tag{38}$$

Let us define the function

$$f(R_1(\mathbf{p}), \dots, R_M(\mathbf{p})) = \frac{1}{\left(\Pi_{m=1}^{M} R_m(\mathbf{p})\right)^{1/M}}. \tag{39}$$

As a result, (38) is equivalent to

$$\begin{aligned} \mathbf{p}^{\text{opt}} = \min_{\{\mathbf{p}\}} & f(R_1(\mathbf{p}), \dots, R_M(\mathbf{p})) \\ & \text{s.t. } I_{\text{PU}} \leq I_{\text{th}}, \\ & \|\mathbf{F}_{\text{RF}}\mathbf{F}_{\text{BB}}\mathcal{D}(\sqrt{\mathbf{p}})\|_F^2 \leq P_{\max}. \end{aligned} \tag{40}$$

Let $\mathbf{p}^{\{k\}}$ denote the optimal power obtained in the $(k-1)$th iteration. The linearized form of $f(R_1(\mathbf{p}), \dots, R_M(\mathbf{p}))$ at $(R_1(\mathbf{p}^{\{k\}}), \dots, R_M(\mathbf{p}^{\{k\}}))$ can be written as

$$\begin{aligned} & 2f(R_1(\mathbf{p}^{\{k\}}), \dots, R_M(\mathbf{p}^{\{k\}})) - \\ & f(R_1(\mathbf{p}^{\{k\}}), \dots, R_M(\mathbf{p}^{\{k\}})) \frac{1}{M} \sum_{m=1}^{M} \frac{R_m(\mathbf{p})}{R_m(\mathbf{p}^{\{k\}})}. \end{aligned} \tag{41}$$

Note that $f(R_1(\mathbf{p}^{\{k\}}), \dots, R_M(\mathbf{p}^{\{k\}})) > 0$. Hence, the resultant optimization problem can be written as

$$\begin{aligned} \mathbf{p}^{\text{opt}} = \max_{\mathbf{p}} & \sum_{m=1}^{M} \delta_m^{\{k\}} R_m(\mathbf{p}) \\ & \text{s.t. } I_{\text{PU}} \leq I_{\text{th}}, \\ & \|\mathbf{F}_{\text{RF}}\mathbf{F}_{\text{BB}}\mathcal{D}(\sqrt{\mathbf{p}})\|_F^2 \leq P_{\max}, \end{aligned} \tag{42}$$

where $\delta_m^{\{k\}} = \frac{f(R_1(\mathbf{p}^{\{k\}}),\ldots,R_M(\mathbf{p}^{\{k\}}))}{R_m(\mathbf{p}^{\{k\}})}, \forall m$. To solve the above problem one can use the steepest descent procedure to generate the next feasible point ($\mathbf{p}^{\{k+1\}}$), given as

Theorem 2.

$$p_m^{\{k+1\}} = \begin{cases} \delta_m^{\{k\}}(\mathbf{N}^{\{k\}})^{-1}\mathbf{b}_m^{\{k\}}, \text{ if } \sum_{m=1}^{M}(\mathrm{diag}(\hat{\mathbf{Z}}_m))^H\delta_m^{\{k\}} \\ \times(\mathbf{N}^{\{k\}})^{-1}\mathbf{b}_m^{\{k\}} \leq I_{\mathrm{th}} \text{ and} \\ \sum_{m=1}^{M}(\mathrm{diag}(\hat{\mathbf{T}}_m))^H\delta_m^{\{k\}}(\mathbf{N}^{\{k\}})^{-1}\mathbf{b}_m^{\{k\}} \leq P_{\max} \\ \delta_m^{\{k\}}\left(\mathbf{N}^{\{k\}} + (\kappa+\nu)\mathbf{I}_{N_\mathrm{s}}\right)^{-1}\mathbf{b}_m^{\{k\}}, \qquad \text{otherwise} \end{cases} \tag{43}$$

where $\kappa > 0$ and $\nu > 0$ are found by bisection method such that $\sum_{m=1}^{M}(\mathrm{diag}(\hat{\mathbf{Z}}_m))^H\delta_m^{\{k\}}(\mathbf{N}^{\{k\}}+\kappa\mathbf{I}_{N_\mathrm{s}})^{-1}\mathbf{b}_m^{\{k\}} = I_{\mathrm{th}}$ and $\sum_{m=1}^{M}(\mathrm{diag}(\hat{\mathbf{T}}_m))^H\delta_m^{\{k\}}(\mathbf{N}^{\{k\}} + \nu\mathbf{I}_{N_\mathrm{s}})^{-1}\mathbf{b}_m^{\{k\}} = P_{\max}$.

Proof. Given in Appendix C. □

Therefore, the optimal power allocation is found by repeating the update in (43) till the objective function of (38) converges. The proposed two-stage hybrid TPC design and power allocation at the CBS has the following complexity. With the aid of [4], the complexity of Step 1 in Algorithm 2 may be shown to be on the order $\mathcal{O}(N_\mathrm{t}^2 M_\mathrm{t} N_\mathrm{s})$, while Step 2 and Step 3 involve a pseudo inverse computation and matrix multiplication that have complexities of $\mathcal{O}(MN_\mathrm{s}^4)$ and $\mathcal{O}\left[M_\mathrm{t}N_\mathrm{s}\left(2N_\mathrm{s}-1\right)\right]$, respectively. Furthermore, the power allocation schemes based on Theorem 1 and Theorem 2 iterate using the closed-form expressions in (37) and (43), respectively, which results in a very low complexity compared to Algorithm 2. As a result, the overall complexity order of the TPC design, along with optimal power allocation at the CBS, is $\mathcal{O}(N_\mathrm{t}^2 M_\mathrm{t} N_\mathrm{s})$.

It is worth noting that the two-stage hybrid TPC design developed in this section explicitly assumes that the CBS has perfect knowledge of each SU's channel $\mathbf{H}_m$ and hybrid RC matrices $\mathbf{W}_{\mathrm{RF},m}, \mathbf{W}_{\mathrm{BB},m}, \forall m$. Hence, the CBS is able to calculate $\mathbf{F}_{\mathrm{opt}}$ in the first stage and designs $\mathbf{F}_{\mathrm{BB}}^2$ via the ZF technique in the second stage using the perfect knowledge of $\widetilde{\mathbf{H}}_m^{\mathrm{eff}}$, which is challenging, if not impossible, to obtain in practical systems. Therefore, the next section overcomes this impediment via limited feedback.

V. PRECODING/COMBINING IN LIMITED FEEDBACK

This paper proposes the design of the RF RCs $\mathbf{W}_{\mathrm{RF},m}$ using a quantized codebook, which is well-suited for limited feedback, since their columns can be represented using the corresponding indices of the $N_\mathrm{r}-$dimensional DFT codebook $\mathbf{G}_{\mathrm{Rx}}$. This requires $\log_2 N_\mathrm{r}$ bits for representing each column of $\mathbf{W}_{\mathrm{RF},m}$, implying that $M_\mathrm{r}\log_2 N_\mathrm{r}$ bits are required for the limited feedback of $\mathbf{W}_{\mathrm{RF},m}$. However, the techniques described in the above sections consider analog feedback of the mmWave MIMO channel $\mathbf{H}_m$ and baseband RC $\mathbf{W}_{\mathrm{BB},m}$. This can be avoided following the limited feedback approach described below:

(i) With the knowledge of the mmWave MIMO channel $\mathbf{H}_m$, each SU performs blind MMSE RC as discussed in Section III along with some modifications explained next. It follows from the design of $\mathbf{W}_{\mathrm{RF},m}$ that it satisfies the property $\mathbf{W}_{\mathrm{RF},m}^H\mathbf{W}_{\mathrm{RF},m} = \mathbf{I}_{M_\mathrm{r}}$. Furthermore, we additionally restrict the baseband RC $\mathbf{W}_{\mathrm{BB},m}$ in (23) to be semi-unitary, i.e., $\mathbf{W}_{\mathrm{RF},m}^H\mathbf{W}_{\mathrm{BB},m}^H\mathbf{W}_{\mathrm{BB},m}\mathbf{W}_{\mathrm{RF},m} = \mathbf{I}_{N_\mathrm{s}}$. Note that this design constraint implies that the noise covariance matrix $\mathbf{R}_{\mathrm{nn},m}$ at the output of the RC in (25) reduces to $\sigma^2\mathbf{I}_{N_\mathrm{s}}$, which significantly reduces the feedback overhead required, since now one does not have to feed back the RF and BB RCs $\mathbf{W}_{\mathrm{RF},m}, \mathbf{W}_{\mathrm{BB},m}\forall m$, respectively, to the CBS. This enables the CBS to design the hybrid TPCs using only the effective channel $\widetilde{\mathbf{H}}_m = \mathbf{W}_{\mathrm{BB},m}^H\mathbf{W}_{\mathrm{RF},m}^H\mathbf{H}_m$. This additional semi-unitary constraint on the baseband RC $\mathbf{W}_{\mathrm{BB},m}$ can be supported by replacing the least squares solution in step (7) of Algorithm 1, by the solution to the corresponding (OPP) [34]. This is given by $\mathbf{W}_{\mathrm{BB},m} = \mathbf{U}_{m1}\mathbf{V}_{m1}^H$, where $\mathbf{U}_{m1} \in \mathbb{C}^{M_\mathrm{r}\times N_\mathrm{s}}$ and $\mathbf{V}_{m1} \in \mathbb{C}^{N_\mathrm{s}\times N_\mathrm{s}}$ are unitary matrices obtained from the compact SVD of the quantity $\mathbf{W}_{\mathrm{RF},m}^H\mathbf{R}_{\bar{\mathrm{y}}\bar{\mathrm{y}},m}\mathbf{W}_{\mathrm{MMSE},m}$.

(ii) Finally, each SU quantizes the effective channel matrix $\widetilde{\mathbf{H}}_m$ using a RVQ codebook, and feeds the corresponding index of each quantized channel vector back to the CBS using a limited number of bits. The finer details of RVQ codebook design are omitted here due to space constraints. However, the construction procedure of such a codebook has been well-studied in the rich literature on limited feedback MIMO systems in [35], [36], [37], which can be referred by the interested readers.

Toward quantization, the normalized channel matrix of the mth SU is obtained as $\hat{\mathbf{H}}_m = \frac{\widetilde{\mathbf{H}}_m}{||\widetilde{\mathbf{H}}_m||_F} = [\hat{\mathbf{h}}_{m,1},\ldots,\hat{\mathbf{h}}_{m,N_\mathrm{t}}]$. Next, using an RVQ codebook $\mathcal{H}$ of size 2^B, the quantized vectors $\hat{\mathbf{h}}_{m,i}, \forall i$ are choosen such that

$$\hat{\mathbf{h}}_{m,i}^{\mathbf{Q}} = \underset{\mathbf{g}\in\mathcal{H}}{\arg\max}\,|(\hat{\mathbf{h}}_{m,i})^H\mathbf{g}|, i = 1,\ldots,N_\mathrm{t} \tag{44}$$

to obtain the quantized matrix $\hat{\mathbf{H}}_m^{\mathbf{Q}} = [\hat{\mathbf{h}}_{m,1}^Q,\ldots,\hat{\mathbf{h}}_{m,N_\mathrm{t}}^Q]$. Furthermore, the CBS uses Algorithm 2 to design the TPC based on $\hat{\mathbf{H}}_m^{\mathbf{Q}}$ followed by optimal power allocation using Theorem 1 and Theorem 2 toward sum SE and GM maximization, respectively.

Let R_m^{Q} denote the resulting rate of the mth SU achieved via this limited feedback procedure. As a result, the average rate loss per SU $\overline{\Delta R}_m$ can be defined as

$$\overline{\Delta R}_m = \mathbb{E}[R_m - R_m^{\mathrm{Q}}], \tag{45}$$

which can be upper-bounded by following [3] as

$$\begin{aligned}\overline{\Delta R}_m \leq \log_2 \Bigg| \mathbf{I}_{N_\mathrm{s}} + \frac{\overline{\alpha}}{\sigma^2}N_\mathrm{t}N_\mathrm{r}2^{-\frac{B}{M_\mathrm{t}-1}} \\ \times\left(1+\frac{M_\mathrm{t}-1}{N_\mathrm{t}}\left(1+\frac{N_\mathrm{p}-1}{N_\mathrm{t}N_\mathrm{r}}\right)\right)\mathcal{D}(\mathbf{p}_m)\Bigg|,\end{aligned} \tag{46}$$

with $\overline{\alpha} = \mathbb{E}[|\alpha_{m,l}|^2], \forall m,l$.

In the large antenna regime, $\frac{N_\mathrm{p}-1}{N_\mathrm{t}N_\mathrm{r}} \ll 1$ and $\frac{M_\mathrm{t}-1}{N_\mathrm{t}} \ll 1$.

Therefore, in such a system, (46) reduces to

$$\overline{\Delta R}_m \leq \log_2 \left| \mathbf{I}_{N_\mathrm{s}} + \frac{\overline{\alpha}}{\sigma^2} N_\mathrm{t} N_\mathrm{r} 2^{-\frac{B}{M_\mathrm{t}-1}} \mathcal{D}(\mathbf{p}_m) \right|. \tag{47}$$

One can observe from 47 that the rate loss is proportional to the number of TAs/RAs and the number of RF chains.

VI. SIMULATION RESULTS

This section presents our simulation results for demonstrating the performance of the blind MMSE hybrid RC approach followed by the proposed 2-stage hybrid TPC method to maximize the sum SE and GM of SU rates for mmWave MU MIMO CR systems. We compare the results obtained to that of the EGT-BD (equal gain transmission-block diagonalization) design technique proposed in [28], the fully analog technique of [25], hybrid transmit beamforming technique of [26], and also benchmark them using the performance of an ideal fully digital beamformer. Note that the techniques proposed in [25] and [26] are designed for single-RF chain based systems. Hence, they require MN_s time slots for transmission of MN_s data symbols, resulting in MUI- and ISI-free transmission. Moreover, the simulation setup comprises a uniform linear array (ULA) configuration with half-wavelength antenna spacing for the CBS and all the SUs. The mmWave MIMO channel has $N_p = 10$ multipath components for which the AoA/AoDs are assumed to follow a uniform distribution between $[0, 2\pi]$. While implementing the SOMP based TPC/RC algorithm, this work further considers two scenarios:

(i) the availability of perfect knowledge of the antenna array steering vectors at each SU and CBS. This is a hypothetical scenario and its performance serves purely as a bound.

(ii) A realistic scenario, where the antenna array steering vectors are unknown to all the SUs and CBS. In this scenario, the mth SU and CBS employ predetermined codebooks for designing $\mathbf{W}_{\mathrm{RF},m}, \forall m$, and $\mathbf{F}_\mathrm{RF}$ respectively. For this purpose, at each SU, an $N_\mathrm{r}-$dimensional DFT basis is considered as the codebook $\mathbf{G}_\mathrm{Rx}$, whereas an over-complete codebook $\mathbf{G}_\mathrm{Tx}$ with size $N_\mathrm{t} \times 2N_\mathrm{t}$ is employed at the CBS.

Furthermore, in line with the existing mmWave MU MIMO literature, this work considers the number of RF chains at CBS to be equal to the sum of the number of all RF chains at all the SUs i.e., $M_\mathrm{t} = MM_\mathrm{r}$. The range of the maximum tolerable interference level I_th of the PU is kept between -10 dB to 25 dB to examine the system performance in both the low as well as high I_th regime, whereas the maximum available transmit power P_max at the CBS is set to 10 dB. Finally, all the reported simulation results are obtained by averaging over 1000 random mmWave MIMO channel realizations.

Fig. 3 shows the SE achieved by an 8×128 system for $N_\mathrm{s} = 2$ and $N_\mathrm{s} = 4$ data streams, where the number of antennas at each SU is $N_\mathrm{r} = 8$ and that at the CBS is $N_\mathrm{t} = 128$. The CBS is equipped with $M_\mathrm{t} = MM_\mathrm{r}$ RF chains for serving $M = 8$ SUs, each having $M_\mathrm{r} = 2N_\mathrm{s}$ RF chains. One can observe from the figure that there is a net loss in SE from GM maximization in comparison with the sum SE maximization, which can be treated as the cost required to achieve user fairness. However, the proposed hybrid transceiver design for our MU CR system approaches the SE of the optimal fully-digital solution for $N_\mathrm{s} = 2$ data streams per SU. By contrast, for $N_\mathrm{s} = 4$, there is a slight SE gap achieved with respect to the ideal fully-digital architecture. This can be attributed jointly to the increased error in approximating the hybrid TPC to the ideal fully-digital TPC as well as the increased ISI. It is also important to note that the proposed design using codebooks is closely capable of tracking the performance of the scenario, where perfect knowledge of the antenna array steering vectors is available. This demonstrates the efficacy of the codebooks employed and also relaxes the requirement of perfect knowledge of the array steering vectors at the respective ends. One can note that for a low interference threshold I_th, the performance achieved by EGT-BD closely resembles the performance achieved by the proposed design. However, for a high I_th, its performance degrades significantly. This is due to the inability of the EGT-BD to cancell the resultant ISI at high values of I_th, which arises due to the suboptimal nature of the BD method. However, the schemes described in [25] and [26] lag behind the proposed scheme due to the lack of available degrees of freedom, whereas the proposed scheme exploits multi-stream communication at both the CBS and each SU in a single time slot.

To further explore the performance in a MU mmWave MIMO CR system relying on large antenna arrays, Fig. 4 plots the SE attained for a 16×256 system, where the CBS is equipped with $M_\mathrm{t} = 64$ RF chains for serving $M = 8$ secondary users, each having $M_\mathrm{r} = 8$ RF chains. A similar trend is observed here, where the proposed design using codebooks performs very close to the benchmarks. One can also note the improved SE upon increasing the dimensions of the system from 8×128 to 16×256, which is due to the dual effects of a higher beamforming gain and combined with the increased rank of the effective baseband channel. Fig. 5 shows the SE versus interference threshold I_th by considering $M_r \in \{4, 8, 10\}$ RF chains at each SU and the corresponding RF chains at the CBS, so that we have $M_\mathrm{t} = MM_\mathrm{r}$ for a fixed number of data streams $N_\mathrm{s} = 4$. It can be seen from the figure that the SE of both sum SE and GM maximization using the proposed design procedures approach that of the optimal fully digital design upon increasing M_r. This is because, upon increasing the number of RF chains, the RF TPC $\mathbf{F}_\mathrm{RF}$ and the RCs $\mathbf{W}_{\mathrm{RF},m}$ comprise an increased number of columns from the corresponding codebooks, which leads to a reduced approximation error in (18) and (27). Note that in the CR system, there is a power limitation at the SUs due to the resultant interference threshold at the PU. Hence it is desirable to increase the number of RF chains at the CBS, which will lead to an increased of overall SE, while compensating for the limited power.

The SE of the system is further investigated by altering its multiplexing settings, i.e. the number of parallel data streams

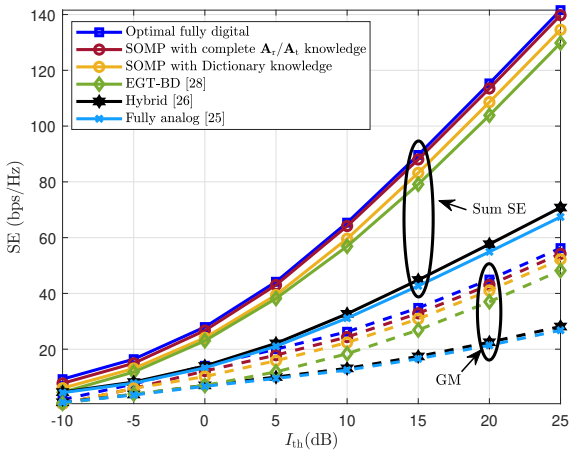

(a) $N_{\text{s}} = 2$

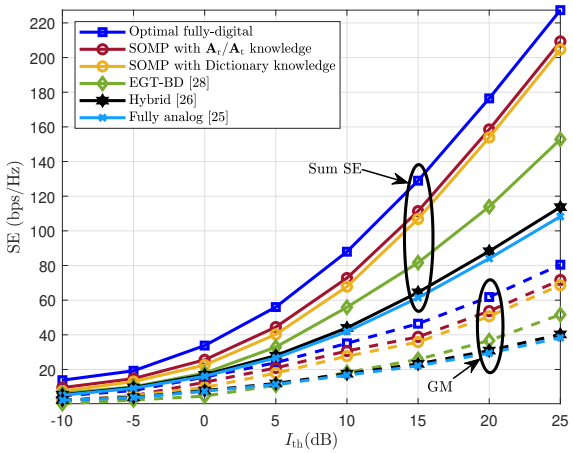

(b) $N_{\text{s}} = 4$

Figure 3: SE versus I_{th} of different TPC/RC solutions for a 8×128 mmWave MU MIMO CR system with $M = 8, M_{\text{r}} = 2N_{\text{s}}, M_{\text{t}} = MM_{\text{r}}$.

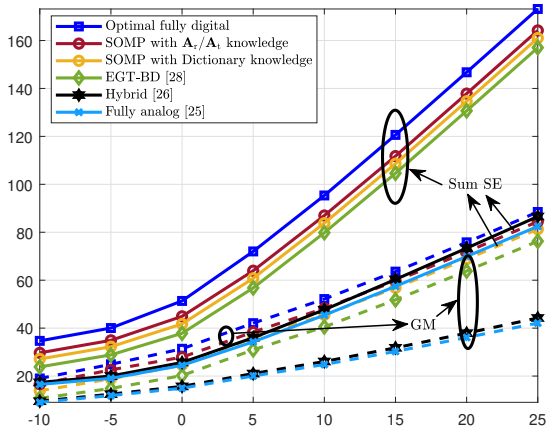

(a) $N_{\text{s}} = 2$

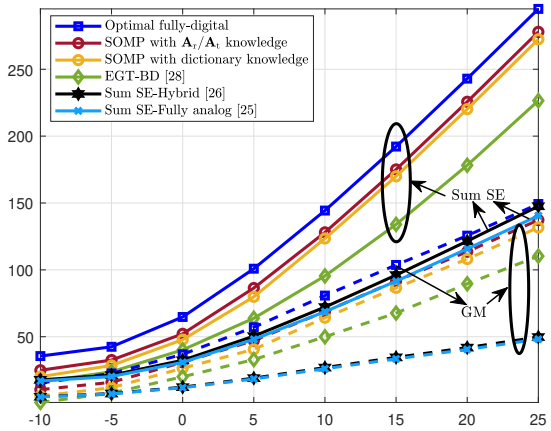

(b) $N_{\text{s}} = 4$

Figure 4: SE versus I_{th} of different TPC/RC solutions for a 16×256 mmWave MU MIMO CR system with $M = 8, M_{\text{r}} = 2N_{\text{s}}, M_{\text{t}} = MM_{\text{r}}$.

N_{s} handled by each SU, and the number of SUs M supported by the CBS at any given moment, since the total number of supported data streams is dependent on the number of SUs supported by CBS and the number of parallel data streams supported by each SU. Fig. 6 and Fig. 7 illustrate the SE achieved by different TPC/RC solutions in a 16×256 system for interference threshold $I_{\text{th}} = 5$ dB. The number of serving SUs is varied from $M = 2$ to 14. The number of data streams per SU is set to $N_{\text{s}} = 2$ for Fig. 6, whereas it is kept as $N_{\text{s}} = 4$ for Fig. 7. Observe from both figures that the SE of both sum SE and GM using the proposed scheme increases upon increasing number of SUs M, and the number of streams N_{s}. On the other hand, the SE of the EGT-BD saturates and beyond $M = 10$ it degrades upon increasing N_{s} and M due to the significant overlap of the row subspaces of the channels $\mathbf{H}_m$, which reduces its capability of cancelling the MUI and ISI [29]. Furthermore, the gap between the SE of the proposed scheme with respect to the fully-digital benchmark increases for $N_{\text{s}} = 4$, since in this scenario the approximation error defined in Eq. (27) increases, ultimately leading to an increase in the MUI. On the other hand, one can see that the gap between the proposed scheme and EGT-BD increases upon increasing N_{s} and M, which shows the efficiency of the ZF method used in the second stage of designing the TPC $\mathbf{F}_{\text{BB}}^2$. Fig. 8 compares the SE achieved by the different TPC/RC solutions, when the number of CBS antennas N_{t} is varied from 128 to 512 for a fixed number of RF chains $M_{\text{t}} = 32$ at the CBS. The number of SUs M is set to 8, each equipped with $N_{\text{r}} = 8$ antennas and $M_{\text{r}} = 4$ RF chains. Furthermore, the performance is evaluated at $I_{\text{th}} = 5$ dB prescribed by the

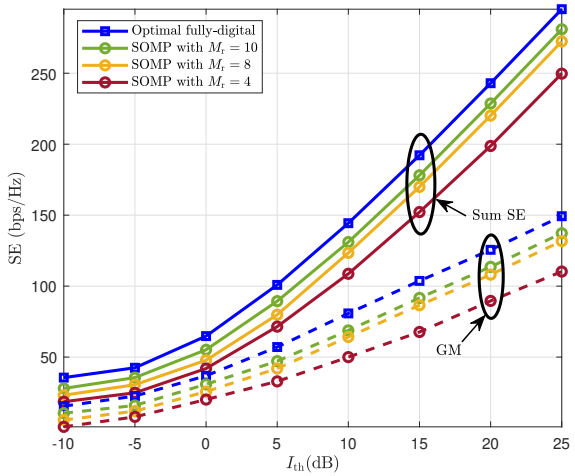

Figure 5: SE versus I_{th} of proposed TPC/RC solutions for a 16×256 mmWave MU MIMO CR system with $M = 8$ and for different values of M_{r} at each SU with $N_{\text{s}} = 4$.

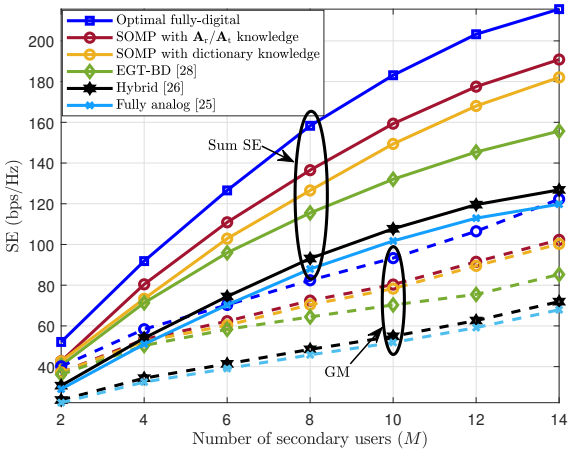

Figure 7: SE attained by different TPC/RC solutions in a 16×256 mmWave MU MIMO CR system where M increases from 2 to 14, $I_{\text{th}} = 5$ dB and N_{s}=4.

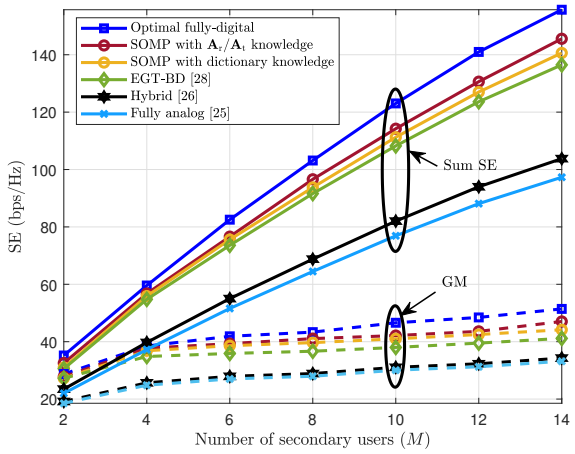

Figure 6: SE attained by different TPC/RC solutions in a 16×256 mmWave MU MIMO CR system where M increases from 2 to 14, $I_{\text{th}} = 5$ dB and N_{s}=2.

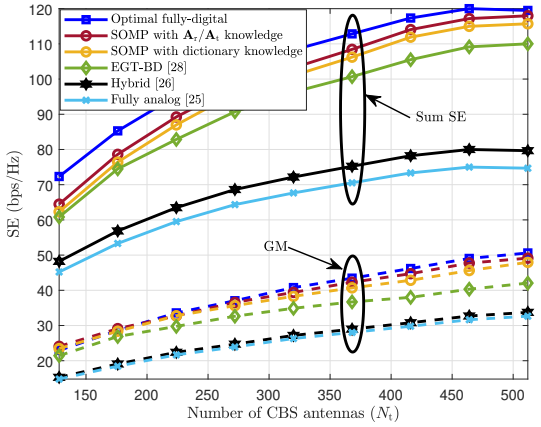

Figure 8: SE attained by different TPC/RC solutions where the number of CBS antennas (N_{t}) varies from 128 to 512, $N_{\text{r}} = 8$,$M = 8$, $I_{\text{th}} = 5$ dB and N_{s}=2.

PU. The figure shows that as the number of CBS antennas N_{t} increases, the SEs of the sum and GM rate maximization paradigms for the various TPC designs improves as a result of the ensuing beamforming gain. It can be readily observed that the proposed scheme outperforms its existing counterpart. Furthermore, when the number of CBS antennas N_{t} increases, the performance gap between the proposed design and the EGT-BD increases. At the same time, the SE of the proposed scheme approaches that of the ideal fully-digital transceiver upon increasing N_{t}. This finding suggests that for improving the SE, one can increase the number of CBS antennas instead of increasing the number of power-hungry RF chains.

Finally, Fig. 9 and Fig. 10 plot the SE achieved by the proposed TPC/RC solution for the 8×128 and 16×256 downlink mmWave MU MIMO CR systems considered in Fig. 3 and Fig. 4, respectively, but for the limited feedback scenario of Section V. Furthermore, we assume that each SU uses $B = 4$ bits to quantize the columns of the effective channel matrix in both 8×128 and 16×256 systems. Observe from the figure that the effective channel matrix $\widetilde{\mathbf{H}}_m$ and its limited feedback leads to some loss in the SE of both the sum and GM rate maximization approaches. However, upon increasing the number of antennas, both sum SE and GM performance degrades as compared with analog feedback as shown in Fig. 10. This is because the rate loss increases logarithmically with the antenna numbers as shown in (47). Therefore, one should increase the number of quantization bits with the antennas numbers to avoid the significant performance degradation. Thus, there is a trade-off between the SE and feedback overhead.

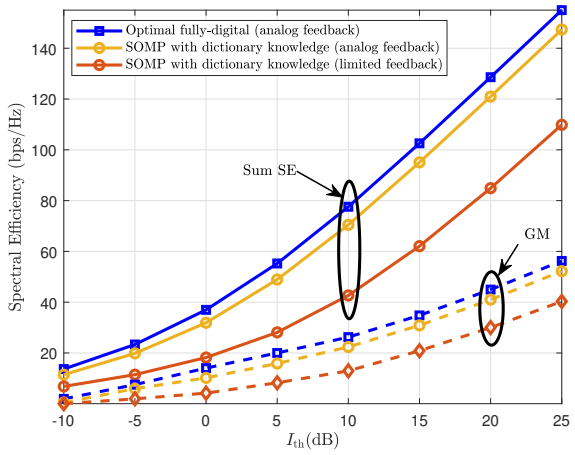

Figure 9: SE versus I_{th} of proposed TPC/RC solutions with limited feedback for 8×128 mmWave MU MIMO CR systems with $N_{\text{s}}=2, B=4$.

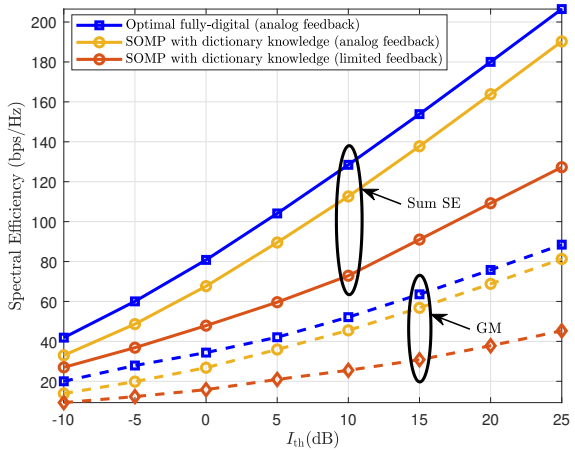

Figure 10: SE versus I_{th} of proposed TPC/RC solutions with limited feedback for 16×256 mmWave MU MIMO CR systems with $N_{\text{s}}=2, B=4$.

VII. CONCLUSION

Hybrid TPC and RC designs were conceived for the downlink of a MU mmWave MIMO CR system operating in the underlay mode. Decoupled hybrid TPC, MMSE-RC and optimal power allocation solutions were presented that either maximize the overall downlink SE of the SUs or GM of the SU rates, while satisfying the interference constraint imposed by the PU. A limited feedback strategy relying on OPP and RVQ was also developed, which significantly reduces the overhead, while performing close to its analog feedback counterpart. Our simulation results demonstrated that the proposed scheme can achieve a performance comparable to that of ideal fully-digital beamforming, while outperforming the existing techniques, which can be attributed to the efficient nature of the low-complexity ZF-based MUI cancellation procedure. Furthermore, it has been observed that the performance gap between the proposed technique and the fully-digital benchmark reduces upon increasing the system dimensions, i.e., number of TAs/RAs and RF chains. It would be interesting to develop the corresponding transceiver design for frequency-selective mmWave MIMO systems in our future work.

APPENDIX A
DERIVATION FOR EQ. (26)

Using the SVD of $\widetilde{\mathbf{H}}_m$, (25) can be written as

$$\mathcal{R}_m = \log_2\left(\left|\mathbf{I}_{N_{\text{s}}} + \mathbf{R}^{-1}_{\tilde{\text{n}},m}\widetilde{\mathbf{U}}_m\widetilde{\mathbf{\Sigma}}_m\widetilde{\mathbf{V}}_m^H\mathbf{F}_{\text{RF}}\mathbf{F}^1_{\text{BB},m}\mathbf{F}^2_{\text{BB},m} \times\mathcal{D}(\mathbf{p}_m)(\mathbf{F}^2_{\text{BB},m})^H(\mathbf{F}^1_{\text{BB},m})^H\mathbf{F}^H_{\text{RF}}\widetilde{\mathbf{V}}_m\widetilde{\mathbf{\Sigma}}_m^H\widetilde{\mathbf{U}}_m^H\right|\right).$$

Furthermore, let us define the following two partitions of the matrices $\widetilde{\mathbf{\Sigma}}_m$ and $\widetilde{\mathbf{V}}_m$ as $\widetilde{\mathbf{\Sigma}}_m = \left[\widetilde{\mathbf{\Sigma}}^1_m \;\; \mathbf{0}\right]$ and $\widetilde{\mathbf{V}}_m = [\widetilde{\mathbf{V}}^1_m \;\; \widetilde{\mathbf{V}}^2_m]$, where $\widetilde{\mathbf{\Sigma}}^1_m$ and $\widetilde{\mathbf{V}}^1_m$ are of dimensions $N_{\text{s}}\times N_{\text{s}}$ and $N_{\text{t}}\times N_{\text{s}}$ respectively. Since, the eigenvalues of the matrix $\mathbf{I}_{N_{\text{s}}}-(\widetilde{\mathbf{V}}^1_m)^H\mathbf{F}_{\text{RF}}\mathbf{F}^1_{\text{BB},m}\widetilde{\mathbf{V}}^1_m$ and singular values of the matrix $(\widetilde{\mathbf{V}}^2_m)^H\mathbf{F}_{\text{RF}}\mathbf{F}^1_{\text{BB},m}$ are small, we have $(\widetilde{\mathbf{V}}^1_m)^H\mathbf{F}_{\text{RF}}\mathbf{F}^1_{\text{BB},m}\approx\mathbf{I}_{N_{\text{s}}}$ and $(\widetilde{\mathbf{V}}^2_m)^H\mathbf{F}_{\text{RF}}\mathbf{F}^1_{\text{BB},m}\approx\mathbf{0}$,

$$\begin{aligned}
\mathcal{R}_m &= \log_2\Big(\Big|\mathbf{I}_{N_{\text{s}}} + \mathbf{R}^{-1}_{\text{nn,m}}\widetilde{\mathbf{U}}_m\widetilde{\mathbf{\Sigma}}^1_m(\widetilde{\mathbf{V}}^1_m)^H\mathbf{F}_{\text{RF}}\mathbf{F}^1_{\text{BB},m}\mathbf{F}^2_{\text{BB},m} \\
&\qquad \mathcal{D}(\mathbf{p}_m)(\mathbf{F}^2_{\text{BB},m})^H(\mathbf{F}^1_{\text{BB},m})^H\mathbf{F}^H_{\text{RF}}\widetilde{\mathbf{V}}^1_m(\widetilde{\mathbf{\Sigma}}^1_m)^H\widetilde{\mathbf{U}}_m^H\Big|\Big) \\
&= \log_2\Big(\Big|\mathbf{I}_{N_{\text{s}}} + (\widetilde{\mathbf{\Sigma}}^1_m)^H\widetilde{\mathbf{U}}_m^H\mathbf{R}^{-1}_{\text{nn,m}}\widetilde{\mathbf{U}}_m\widetilde{\mathbf{\Sigma}}^1_m \\
&\qquad \times\underbrace{(\widetilde{\mathbf{V}}^1_m)^H\mathbf{F}_{\text{RF}}\mathbf{F}^1_{\text{BB},m}}_{\approx\mathbf{I}_{N_{\text{s}}}}\mathbf{F}^2_{\text{BB},m}\mathcal{D}(\mathbf{p}_m)(\mathbf{F}^2_{\text{BB},m})^H \\
&\qquad \times\underbrace{(\mathbf{F}^1_{\text{BB},m})^H\mathbf{F}^H_{\text{RF}}\widetilde{\mathbf{V}}^1_m}_{\approx\mathbf{I}_{N_{\text{s}}}}\Big|\Big) \\
&= \log_2\Big(\Big|\mathbf{I}_{N_{\text{s}}} + (\widetilde{\mathbf{\Sigma}}^1_m)^H\widetilde{\mathbf{U}}_m^H\mathbf{R}^{-1}_{\text{nn,m}}\widetilde{\mathbf{U}}_m\widetilde{\mathbf{\Sigma}}^1_m\mathbf{F}^2_{\text{BB},m}\mathcal{D}(\mathbf{p}_m) \\
&\qquad (\mathbf{F}^2_{\text{BB},m})^H(\widetilde{\mathbf{V}}^1_m)^H\mathbf{F}_{\text{RF}}\mathbf{F}^1_{\text{BB},m}(\mathbf{F}^1_{\text{BB},m})^H\mathbf{F}^H_{\text{RF}}\widetilde{\mathbf{V}}^1_m\Big|\Big) \\
&= \log_2\left(\left|\mathbf{I}_{N_{\text{s}}} + \Xi_m\Omega_m\right|\right),
\end{aligned}$$

where $\Xi_m = (\widetilde{\mathbf{\Sigma}}^1_m)^H\widetilde{\mathbf{U}}_m^H\mathbf{R}^{-1}_{\text{nn,m}}\widetilde{\mathbf{U}}_m\widetilde{\mathbf{\Sigma}}^1_m\mathbf{F}^2_{\text{BB},m}\mathcal{D}(\mathbf{p}_m)(\mathbf{F}^2_{\text{BB},m})^H$ and $\Omega_m = (\widetilde{\mathbf{V}}^1_m)^H\mathbf{F}_{\text{RF}}\mathbf{F}^1_{\text{BB},m}(\mathbf{F}^1_{\text{BB},m})^H\mathbf{F}^H_{\text{RF}}\widetilde{\mathbf{V}}^1_m$.

$$\begin{aligned}
\mathcal{R}_m &= \log_2\left(\left|\mathbf{I}_{N_{\text{s}}} + \Xi_m - \Xi_m\left(\mathbf{I}_{N_{\text{s}}} - \Omega_m\right)\right|\right) \\
&= \log_2\Big(\Big|\left(\mathbf{I}_{N_{\text{s}}} + \Xi_m\right)\Big(\mathbf{I}_{N_{\text{s}}} - \left(\mathbf{I}_{N_{\text{s}}} + \Xi_m\right)^{-1}\Xi_m \\
&\qquad \times\left(\mathbf{I}_{N_{\text{s}}} - \Omega_m\right)\Big)\Big|\Big) \\
&= \log_2\Big(\Big|\left(\mathbf{I}_{N_{\text{s}}} + \Xi_m\right)\Big| \\
&\qquad \times\Big|\Big(\mathbf{I}_{N_{\text{s}}} - \left(\mathbf{I}_{N_{\text{s}}} + \Xi_m\right)^{-1}\Xi_m\left(\mathbf{I}_{N_{\text{s}}} - \Omega_m\right)\Big)\Big|\Big) \\
&= \log_2\Big(\left|\left(\mathbf{I}_{N_{\text{s}}} + \Xi_m\right)\right| + \log_2\Big|\Big(\mathbf{I}_{N_{\text{s}}} - \left(\mathbf{I}_{N_{\text{s}}} + \Xi_m\right)^{-1}\Xi_m \\
&\qquad \times\left(\mathbf{I}_{N_{\text{s}}} - \Omega_m\right)\Big)\Big|\Big)
\end{aligned}$$

$$\overset{b}{\approx} \log_2 \left|\left(\mathbf{I}_{N_\mathrm{s}} + \Xi_m\right)\right| - \mathrm{Tr}\Big(\left(\mathbf{I}_{N_\mathrm{s}} + \Xi_m\right)^{-1} \Xi_m \times \left(\mathbf{I}_{N_\mathrm{s}} - \Omega_m\right) \Big)$$
$$\overset{c}{\approx} \log_2 \left|\left(\mathbf{I}_{N_\mathrm{s}} + \Xi_m\right)\right| - \mathrm{Tr}\left(\mathbf{I}_{N_\mathrm{s}} - \Omega_m\right)$$
$$= \log_2 \left(\left| \mathbf{I}_{N_\mathrm{s}} + (\widetilde{\mathbf{\Sigma}}^1_m)^H \widetilde{\mathbf{U}}^H_m \mathbf{R}^{-1}_{\mathrm{nn,m}} \widetilde{\mathbf{U}}_m \widetilde{\mathbf{\Sigma}}^1_m \mathbf{F}^2_{\mathrm{BB},m} \mathcal{D}(\mathbf{p}_m) \times (\mathbf{F}^2_{\mathrm{BB},m})^H \right| \right) - \left(N_\mathrm{s} - \left|\left| (\widetilde{\mathbf{V}}^1_m)^H \mathbf{F}_{\mathrm{RF}} \mathbf{F}^1_{\mathrm{BB},m} \right|\right|^2_F \right)$$
$$= \log_2 \left(\left| \mathbf{I}_{N_\mathrm{s}} + (\mathbf{F}^2_{\mathrm{BB},m})^H (\widetilde{\mathbf{\Sigma}}^1_m)^H \widetilde{\mathbf{U}}^H_m \mathbf{R}^{-1}_{\mathrm{nn,m}} \widetilde{\mathbf{U}}_m \widetilde{\mathbf{\Sigma}}^1_m \times \mathbf{F}^2_{\mathrm{BB},m} \mathcal{D}(\mathbf{p}_m) \right| \right) - \left(N_\mathrm{s} - \left|\left| (\widetilde{\mathbf{V}}^1_m)^H \mathbf{F}_{\mathrm{RF}} \mathbf{F}^1_{\mathrm{BB},m} \right|\right|^2_F \right),$$

where approximation (b) implies that the eigenvalues of $\mathbf{X} = \left(\mathbf{I}_{N_\mathrm{s}} + \Xi_m\right)^{-1} \Xi_m \left(\mathbf{I}_{N_\mathrm{s}} - \Omega_m\right)$ are small. Hence $\log_2\left(|\mathbf{I}_{N_\mathrm{s}} - \mathbf{X}|\right) \approx \log_2\left(1 - \mathrm{Tr}(\mathbf{X})\right) \approx -\mathrm{Tr}(\mathbf{X})$ while (c) follows due to the high SNR.

Appendix B
Proof of Theorem 1

Observe that the maximization of the concave function in (36) is equivalent to minimizing its negative value. Therefore, we minimize the quantity $-\sum_{m=1}^{M}\sum_{d=1}^{N_\mathrm{s}} \log_2\left(1 + \frac{\gamma^2_{m,d}\|\mathbf{f}^{2,(d)}_{\mathrm{BB},m}\|^2}{\sigma^2} p_{m,d}\right)$ using the Karush-Kuhn-Tucker (KKT) framework. Let the Lagrange multipliers λ, ω and $\mu_{m,d} \forall m,d$ be associated with the interference inequality, maximum transmit power inequality and power causality constraints in equation (36), respectively. Thus, the KKT conditions are given as [38]

$$-\frac{\gamma^2_{m,d}\|\mathbf{f}^{2,(d)}_{\mathrm{BB},m}\|^2}{\sigma^2\left(1 + \frac{\gamma^2_{m,d}\|\mathbf{f}^{2,(d)}_{\mathrm{BB},m}\|^2}{\sigma^2} p_{m,d}\right)} + \lambda\zeta_{m,d} + \omega t_{m,d} - \mu_{m,d} = 0 \ \ \forall m,d,$$
$$\lambda\left(I_{\mathrm{th}} - \sum_{m=1}^{M}\sum_{d=1}^{N_\mathrm{s}} p_{m,d}\zeta_{m,d}\right) = 0,$$
$$\omega\left(P_{\max} - \sum_{m=1}^{M}\sum_{d=1}^{N_\mathrm{s}} p_{m,d} t_{m,d}\right) = 0,$$
$$p_{m,d} \geq 0, \mu_{m,d} \geq 0, \mu_{m,d} p_{m,d} = 0 \ \ \forall m,d. \tag{48}$$

From first condition of (48), power profile can be written as

$$p_{m,d} = \max\left\{0, \frac{1}{\lambda\zeta_{m,d} + \omega t_{m,d}} - \frac{\sigma^2}{\gamma^2_{m,d}\|\mathbf{f}^{2,(d)}_{\mathrm{BB},m}\|^2}\right\} \forall m,d. \tag{49}$$

Note that the λ and ω in (49) can be found using the interior point method such that the KKT conditions in (48) are satisfied.

Appendix C
Proof of Theorem 2

Using Eq. (25), it follows that

$$\mathcal{R}_m(\mathbf{p}) = \log_2\left(\left|\mathbf{I}_{N_\mathrm{s}} + \mathbf{A}_m \mathbf{A}^H_m \mathbf{R}^{-1}_{\mathrm{nn},m}\right|\right), \tag{50}$$

where $\mathbf{A}_m = \widetilde{\mathbf{U}}_m \widetilde{\mathbf{\Sigma}}^1_m \mathbf{F}^2_{\mathrm{BB},m} \mathcal{D}(\sqrt{\mathbf{p}_m}) \in \mathbb{C}^{N_\mathrm{s} \times N_\mathrm{s}}$. Now using the inequality in [20], one obtains

$$\log_2\left(\left|\mathbf{I}_{N_\mathrm{s}} + \mathbf{A}_m \mathbf{A}^H_m \mathbf{R}^{-1}_{\mathrm{nn},m}\right|\right) \geq \log_2\left(\left|\mathbf{I}_{N_\mathrm{s}} + \mathbf{A}^{\{k\}}_m (\mathbf{A}^{\{k\}}_m)^H \mathbf{R}^{-1}_{\mathrm{nn},m}\right|\right) - \mathrm{Tr}\left(\mathbf{A}^{\{k\}}_m (\mathbf{A}^{\{k\}}_m)^H \mathbf{R}^{-1}_{\mathrm{nn},m}\right) + 2\Re\{\mathrm{Tr}(\mathbf{R}^{-1}_{\mathrm{nn},m}\mathbf{A}^{\{k\}}_m \mathbf{A}_m)\}$$
$$- \mathrm{Tr}\left(\left(\mathbf{R}^{-1}_{\mathrm{nn},m} - \left(\mathbf{R}_{\mathrm{nn},m} + \mathbf{A}^{\{k\}}_m (\mathbf{A}^{\{k\}}_m)^H\right)^{-1}\right)^H \times \left(\mathbf{A}_m (\mathbf{A})^H_m + \mathbf{R}_{\mathrm{nn},m}\right)\right). \tag{51}$$

Therefore, the above equation yields

$$\mathcal{R}_m(\mathbf{p}) \geq \mathcal{R}^{\{k\}}_m(\mathbf{p}) = a^{\{k\}}_m + 2\Re\{\mathbf{p}^H_m \mathbf{b}^{\{k\}}_m\} - \frac{c^{\{k\}}_m}{\sigma^2}\sum_{n=1}^{M} \mathbf{p}^H_n \mathrm{diag}(\mathbf{\Upsilon}_\mathrm{m}), \tag{52}$$

where

$$a^{\{k\}}_m \overset{a}{\approx} \mathcal{R}_m(\mathbf{p}^{\{k\}}_m) - \mathbf{p}^H_m \mathrm{diag}(\mathbf{\Upsilon}_\mathrm{m}) - \sigma^2 c^{\{k\}}_m,$$
$$\mathbf{b}^{\{k\}}_m \overset{a}{\approx} \Upsilon_m \sqrt{\mathbf{p}_m},$$
$$c^{\{k\}}_m \overset{a}{\approx} \frac{(\mathrm{diag}(\Upsilon_m))^H \mathbf{p}^{\{k\}}_m}{\sigma^2(1 + (\mathrm{diag}(\Upsilon_m))^H \mathbf{p}^{\{k\}}_m)}. \tag{53}$$

The function $\mathcal{R}^{\{k\}}_m(\mathbf{p})$ is seen to be concave quadratic. Therefore, we solve the following convex problem at the kth iteration to generate $\mathbf{p}^{\{k+1\}}$

$$\max_{\mathbf{p}} \ f^{\{k\}}_b(\mathbf{p}) \quad \text{s.t. } I_{\mathrm{PU}} \leq I_{\mathrm{th}}, \ \|\mathbf{F}_{\mathrm{RF}}\mathbf{F}_{\mathrm{BB}}\mathcal{D}(\sqrt{\mathbf{p}})\|^2_F \leq P_{\max}, \tag{54}$$

where

$$f^{\{k\}}_b(\mathbf{p}) = \sum_{m=1}^{M} \delta^{\{k\}}_m R^{\{k\}}_m(\mathbf{p}) = \sum_{m=1}^{M} \delta^{\{k\}}_m a^{\{k\}}_m + 2\sum_{m=1}^{M} \Re\{\delta^{\{k\}}_m \mathbf{p}^H_m \mathbf{b}^{\{k\}}_m\} - \sum_{m=1}^{M} \mathbf{p}^H_m \mathbf{N}^{\{k\}} \mathbf{p}_m, \tag{55}$$

with $\mathbf{0} \preceq \mathbf{N}^{\{k\}} = \sum_{m=1}^{M} \delta^{\{k\}}_m c^{\{k\}}_m \mathbf{\Upsilon}_m$. Using the Lagrangian multiplier method, the next iterative feasible point $\mathbf{p}^{\{k+1\}}_m$ of (54) is given by

$$\mathbf{p}^{\{k+1\}}_m = \delta^{\{k\}}_m (\mathbf{N}^{\{k\}})^{-1} \mathbf{b}^{\{k\}}_m. \tag{56}$$

REFERENCES

[1] I. A. Hemadeh, K. Satyanarayana, M. El-Hajjar, and L. Hanzo, "Millimeter-wave communications: Physical channel models, design considerations, antenna constructions, and link-budget," *IEEE Communications Surveys & Tutorials*, vol. 20, no. 2, pp. 870–913, 2018.

[2] O. E. Ayach, S. Rajagopal, S. Abu-Surra, Z. Pi, and R. W. Heath, "Spatially sparse precoding in millimeter wave MIMO systems," *IEEE Transactions on Wireless Communications*, vol. 13, no. 3, pp. 1499–1513, 2014.

[3] A. Alkhateeb, G. Leus, and R. W. Heath, "Limited feedback hybrid precoding for multi-user millimeter wave systems," *IEEE Transactions on Wireless Communications*, vol. 14, no. 11, pp. 6481–6494, 2015.

[4] Y. Wang and W. Zou, "Low complexity hybrid precoder design for millimeter wave MIMO systems," *IEEE Communications Letters*, vol. 23, no. 7, pp. 1259–1262, 2019.

[5] A. A. Nasir, H. D. Tuan, T. Q. Duong, H. V. Poor, and L. Hanzo, "Hybrid beamforming for multi-user millimeter-wave networks," *IEEE Transactions on Vehicular Technology*, vol. 69, no. 3, pp. 2943–2956, 2020.

[6] A. A. Nasir, H. D. Tuan, E. Dutkiewicz, and L. Hanzo, "Finite-resolution digital beamforming for multi-user millimeter-wave networks," *IEEE Transactions on Vehicular Technology*, vol. 71, no. 9, pp. 9647–9662, 2022.

[7] N. T. Nguyen, K. Lee, and H. Dai, "Hybrid beamforming and adaptive RF chain activation for uplink cell-free millimeter-wave massive MIMO systems," *IEEE Transactions on Vehicular Technology*, vol. 71, no. 8, pp. 8739–8755, 2022.

[8] X. Zhou, X. Zhang, C. Chen, Y. Niu, Z. Han, H. Wang, C. Sun, B. Ai, and N. Wang, "Deep reinforcement learning coordinated receiver beamforming for millimeter-wave train-ground communications," *IEEE Transactions on Vehicular Technology*, vol. 71, no. 5, pp. 5156–5171, 2022.

[9] F. Hu, B. Chen, and K. Zhu, "Full spectrum sharing in cognitive radio networks toward 5G: A survey," *IEEE Access*, vol. 6, pp. 15 754–15 776, 2018.

[10] Q. Zhang, K. An, X. Yan, and T. Liang, "Coexistence and performance limits for the cognitive broadband satellite system and mmWave cellular network," *IEEE Access*, vol. 8, pp. 51 905–51 917, 2020.

[11] C. Vrontos, F. Boccardi, S. Armour, E. Mellios, and J. Butler, "Performance evaluation of spectrum sharing in mmWave cellular networks using ray-tracing," in *2020 IEEE Wireless Communications and Networking Conference (WCNC)*, 2020, pp. 1–6.

[12] T. A. Tsiftsis, G. Ding, Y. Zou, G. K. Karagiannidis, Z. Han, and L. Hanzo, "Guest editorial spectrum sharing and aggregation for future wireless networks, part iii," *IEEE Journal on Selected Areas in Communications*, vol. 35, no. 1, pp. 1–5, 2017.

[13] F. Boccardi, H. Shokri-Ghadikolaei, G. Fodor, E. Erkip, C. Fischione, M. Kountouris, P. Popovski, and M. Zorzi, "Spectrum pooling in mmWave networks: Opportunities, challenges, and enablers," *IEEE Communications Magazine*, vol. 54, no. 11, pp. 33–39, 2016.

[14] M. Rebato, F. Boccardi, M. Mezzavilla, S. Rangan, and M. Zorzi, "Hybrid spectrum sharing in mmWave cellular networks," *IEEE Transactions on Cognitive Communications and Networking*, vol. 3, no. 2, pp. 155–168, 2017.

[15] R. Jurdi, A. K. Gupta, J. G. Andrews, and R. W. Heath, "Modeling infrastructure sharing in mmWave networks with shared spectrum licenses," *IEEE Transactions on Cognitive Communications and Networking*, vol. 4, no. 2, pp. 328–343, 2018.

[16] C. Fan, B. Li, C. Zhao, W. Guo, and Y.-C. Liang, "Learning-based spectrum sharing and spatial reuse in mm-wave ultradense networks," *IEEE Transactions on Vehicular Technology*, vol. 67, no. 6, pp. 4954–4968, 2017.

[17] H. S. Ghadikolaei, H. Ghauch, G. Fodor, M. Skoglund, and C. Fischione, "A hybrid model-based and data-driven approach to spectrum sharing in mmWave cellular networks," *IEEE Transactions on Cognitive Communications and Networking*, vol. 6, no. 4, pp. 1269–1282, 2020.

[18] S. Sarkar, X. Zhang, A. Bhuyan, M. Ji, and S. K. Kasera, "Uncoordinated spectrum sharing in millimeter wave networks using carrier sensing," *IEEE Transactions on Wireless Communications*, 2022.

[19] H. Shokri-Ghadikolaei, F. Boccardi, C. Fischione, G. Fodor, and M. Zorzi, "Spectrum sharing in mmWave cellular networks via cell association, coordination, and beamforming," *IEEE Journal on Selected Areas in Communications*, vol. 34, no. 11, pp. 2902–2917, 2016.

[20] H. Yu, H. D. Tuan, E. Dutkiewicz, H. V. Poor, and L. Hanzo, "Maximizing the geometric mean of user-rates to improve rate-fairness: Proper vs. improper gaussian signaling," *IEEE Transactions on Wireless Communications*, vol. 21, no. 1, pp. 295–309, 2022.

[21] J. Park, J. G. Andrews, and R. W. Heath, "Inter-operator base station coordination in spectrum-shared millimeter wave cellular networks," *IEEE Transactions on Cognitive Communications and Networking*, vol. 4, no. 3, pp. 513–528, 2018.

[22] J. Jeon, R. D. Ford, V. V. Ratnam, J. Cho, and J. Zhang, "Coordinated dynamic spectrum sharing for 5G and beyond cellular networks," *IEEE Access*, vol. 7, pp. 111 592–111 604, 2019.

[23] A. K. Gupta, J. G. Andrews, and R. W. Heath, "On the feasibility of sharing spectrum licenses in mmWave cellular systems," *IEEE Transactions on Communications*, vol. 64, no. 9, pp. 3981–3995, 2016.

[24] A. K. Gupta, A. Alkhateeb, J. G. Andrews, and R. W. Heath, "Gains of restricted secondary licensing in millimeter wave cellular systems," *IEEE Journal on Selected Areas in Communications*, vol. 34, no. 11, pp. 2935–2950, 2016.

[25] M. A. Vazquez, L. Blanco, A. Perez-Neira, and M. A. Lagunas, "Phase-only transmit beamforming for spectrum sharing microwave systems," in *WSA 2016; 20th International ITG Workshop on Smart Antennas*, 2016, pp. 1–7.

[26] M. A. Vázquez, L. Blanco, and A. I. Pérez-Neira, "Hybrid analog-digital transmit beamforming for spectrum sharing backhaul networks," *IEEE Transactions on Signal Processing*, vol. 66, no. 9, pp. 2273–2285, 2018.

[27] C. G. Tsinos, S. Chatzinotas, and B. Ottersten, "Hybrid analog-digital transceiver designs for multi-user MIMO mmWave cognitive radio systems," *IEEE Transactions on Cognitive Communications and Networking*, vol. 6, no. 1, pp. 310–324, 2019.

[28] A. Agrahari and A. K. Jagannatham, "Sum-rate performance of millimeter wave MIMO shared spectrum systems," 2018. [Online]. Available: https://arxiv.org/submit/4650692/view

[29] W. Ni and X. Dong, "Hybrid block diagonalization for massive multiuser MIMO systems," *IEEE Transactions on Communications*, vol. 64, no. 1, pp. 201–211, 2015.

[30] P. Wang, B. Di, and L. Song, "Cellular communications over unlicensed mmWave bands with hybrid beamforming," *IEEE Transactions on Wireless Communications*, 2022.

[31] Z. Kong, J. Song, C. Wang, H. Chen, and L. Hanzo, "Hybrid analog-digital precoder design for securing cognitive millimeter wave networks," *IEEE Transactions on Information Forensics and Security*, vol. 16, pp. 4019–4034, 2021.

[32] X. Wu, J. Ma, C. Gu, X. Xue, and X. Zeng, "Robust secure transmission design for IRS-assisted mmWave cognitive radio networks," *IEEE Transactions on Vehicular Technology*, vol. 71, no. 8, pp. 8441–8456, 2022.

[33] S. M. Kay, *Fundamentals of Statistical Signal Processing: Estimation Theory*. USA: Prentice-Hall, Inc., 1993.

[34] J. C. Gower and G. B. Dijksterhuis, *Procrustes Problems*. Oxford University Press, 2004, vol. 3.

[35] C.-B. Chae, D. Mazzarese, N. Jindal, and R. W. Heath, "Coordinated beamforming with limited feedback in the MIMO broadcast channel," *IEEE Journal on Selected Areas in Communications*, vol. 26, no. 8, pp. 1505–1515, 2008.

[36] D. J. Love, R. W. Heath, V. K. N. Lau, D. Gesbert, B. D. Rao, and M. Andrews, "An overview of limited feedback in wireless communication systems," *IEEE Journal on Selected Areas in Communications*, vol. 26, no. 8, pp. 1341–1365, 2008.

[37] N. Jindal, "MIMO broadcast channels with finite-rate feedback," *IEEE Transactions on Information Theory*, vol. 52, no. 11, pp. 5045–5060, 2006.

[38] S. Boyd, S. P. Boyd, and L. Vandenberghe, *Convex optimization*. Cambridge university press, 2004.

Jitendra Singh (Member, IEEE) received the integrated dual (B.Tech. and M.Tech.) degree in electronics and communication engineering with specialization in wireless communication and networks from Gautam Buddha University, Greater Noida, India, in 2017. He is currently pursuing the Ph.D. degree with the Department of Electrical Engineering, Indian Institute of Technology Kanpur, Kanpur, India. His research interests include Cognitive Radio Networks, mmWave Communication, Intelligent Reflecting Surface (IRS), Integrated Sensing and Communication (ISAC) systems.

Indranil Chatterjee (Member, IEEE) received the B.Tech. degree in Electronics and Communication Engineering (ECE) from Techno India, Salt Lake, India, in 2018. He is currently pursuing an M.S. degree in Electrical Engineering (EE) from the Indian Institute of Technology Kanpur, Kanpur, India, specializing in signal processing, communication, and networks (SPCOM). His research interests include physical layer design of 5G wireless systems, Cognitive Radio system, and mmWave communications.

Suraj Srivastava (Member, IEEE) received the M.Tech. degree in Electronics and Communication Engineering from Indian Institute of Technology Roorkee, India, in 2012, and Ph.D. degree in Electrical Engineering from Indian Institute of Technology Kanpur, Kanpur, India, in 2022. From July 2012 to November 2013, he was employed as a Staff-I systems design engineer with Broadcom Research India Pvt. Ltd., Bangalore, and from November 2013 to December 2015, he was employed as a lead engineer with Samsung Research India, Bangalore where he worked on developing layer-2 of the 3G UMTS/WCDMA/HSDPA modem. His research interests include applications of Sparse Signal Processing in 5G Wireless Systems, mmWave and Tera-Hertz Communication, Orthogonal Time-Frequency Space (OTFS), Joint Radar and Communication (RadCom), Optimization and Machine Learning. He was awarded Qualcomm Innovation Fellowship (QIF) in year 2018 and 2022 from Qualcomm. He was also awarded Outstanding Ph.D. Thesis and Outstanding Teaching Assistant awards from IIT Kanpur.

Abhishek Agrahari (Member, IEEE) received the M.Tech. degree from Indian Institute of Technology Varanasi, India, in 2010, and Ph.D. degree in Electrical Engineering from Indian Institute of Technology Kanpur, Kanpur, India, in 2018. Currently he is working as a Lead Engineer in Radisys Pvt Limited Marathahalli Bangalore. His interests lies in MIMO NR Massive MIMO, Power Control and RAN systems.

Aditya K. Jagannatham (Member, IEEE) received the bachelor's degree from the Indian Institute of Technology, Bombay, and the M.S. and Ph.D. degrees from the University of California, San Diego, CA, USA. From April 2007 to May 2009, he was employed as a Senior Wireless Systems Engineer with Qualcomm Inc., San Diego, CA where he was a part of the Qualcomm CDMA Technologies (QCT) Division. His research interests include next-generation wireless cellular and WiFi networks, with a special emphasis on various 5G technologies, such as massive MIMO, mmWave MIMO, FBMC, NOMA, full duplex, and others. He is currently a Professor with the Electrical Engineering Department, IIT Kanpur, where he also holds the Arun Kumar Chair Professorship. He has been twice awarded the P. K. Kelkar Young Faculty Research Fellowship for excellence in research, the Qualcomm Innovation Fellowship (QInF), the IIT Kanpur Excellence in Teaching Award, the CAL(IT)2 fellowship at the University of California San Diego and the Upendra Patel Achievement Award at Qualcomm.

Lajos Hanzo (http://www-mobile.ecs.soton.ac.uk,https://en.wikipedia.org/wiki/Lajos_Hanzo) (FIEEE'04) received Honorary Doctorates from the Technical University of Budapest and Edinburgh University. He is a Foreign Member of the Hungarian Science-Academy, Fellow of the Royal Academy of Engineering (FREng), of the IET, of EURASIP and holds the IEEE Eric Sumner Field Award.